CAPITAL UNIVERSITY OF SCIENCE AND TECHNOLOGY,
ISLAMABAD

Numerical simulation of MHD mixed convective nanofluid flow over backward facing step with internal heat generation

by

Asifa Ashraf

A thesis submitted in partial fulfillment for the
degree of Master of Philosophy

in the
Faculty of Computing
Department of Mathematics

March 2017

Numerical simulation of MHD mixed convective nanofluid flow over backward facing step with internal heat generation/absorption.

by
Asifa Ashraf
MMT151011

Dr. Shafqat Hussain
(Thesis supervisor)

Dr. Muhammad Sagheer
(Internal Examiner)

Dr.

(External Examiner)

Dr. Muhammad Sagheer

(Head of Department, Mathematics)

Dr. Muhammad Abdul Qadir
(Dean, Faculty of Computing)

DEPARTMENT OF MATHEMATICS
CAPITAL UNIVERSITY OF SCIENCE AND TECHNOLOGY,
ISLAMABAD
March 2017

Certificate of Approval

This is certify that **Asifa Ashraf**, Reg. NO. MMT151011 has incorporated all suggestion, clarification and explanation by the thesis supervisor Dr. Shafqat Hussain as well as external evaluator and internal examiner at Capital University of Science and Technology Islamabad. The research work titled her Thesis is: **Numerical simulation of MHD mixed convective nanofluid flow over backward facing step with internal heat generation.**

Forwarded for necessary action

Dr. Shafqat Hussain

(Thesis supervisor)

Declaration of Authorship

I,"Asifa Ashraf", declare that this thesis titled, 'Numerical simulation of MHD mixed convective nanofluid flow over backward facing step with internal heat generation/absorption' and the work presented in it are my own. I confirm that:

- This work was done completely or mainly while in candidature for a research degree at this University.
- Where any part of this thesis has previously been submitted for a degree or any other qualification at this University or any other institute, this has been clearly stated.
- Where I have consulted the published work of others, this is always been clearly attributed.
- Where I have quoted from the work of others, the sources are always given. With the exception of such quotations, this thesis is entirely my own work.
- I have acknowledged all main sources of help.
- Where the thesis is based on the work, I done by myself jointly with others, I have made clear exactly what was done by others and what I have contributed myself.

Asifa Ashraf
MMT151011

Signed: _____

Date: _____

"Mathematics is the queen of sciences"

Carl. Friedrich Gauss

CAPITAL UNIVERSITY OF SCIENCE AND TECHNOLOGY, ISLAMABAD

Abstract

Faculty of Computing
Department of Mathematics

Master of Philosophy
by
Asifa Ashraf

The aim of this thesis is to focus on a numerical study of laminar mixed convection of nanofluid flow over a backward facing step for different inclination angles of magnetic field with internal heat generation. The bottom wall of the channel downstream of the step is isothermally heated and the other walls of the channel are assumed to be adiabatic. The influence of the heat generation/absorption parameter, Reynolds number, Hartmann number, solid volume fraction of the nanoparticle on the fluid flow and heat transfer are numerically investigated for different orientation angles of the magnetic field. Dimensionless governing equations are discretized by using Galerkin weighted residual method of Finite element formulation. The obtained results are presented in terms of streamlines and isotherms for an inclination angles of magnetic field ranges from 0° to 90°. The results show that the average Nusselt number decreases with the increasing of heat generation parameter. It is also observed that average heat transfer increases with an increase in Reynolds number. Moreover, Nusselt number augments with an enhancement in inclination angle of magnetic field.

Acknowledgements

All the praise and appreciation are for almighty ALLAH who is the most beneficent and the most merciful created the universe and blessed the mankind with Intelligence and wisdom to explore His secrets. Countless respect and endurance for Prophet Muhammad (Peace Be Upon Him), the fortune of knowledge, who took the humanity out of ignorance and shows the right path.

I would like to show my gratitude and immeasurable respect to my supervisor **Dr. Shafqat Hussain**, Associate Professor, Capital University of Science and Technology, Islamabad who suggested the problem, extended all facilities and provided inspiring guidance for the successful completion of my research work. I deem it as my privilege to work under his able guidance.

Special thanks to my teacher **Dr. Muhammad Sagheer**, Associate Professor, Capital University of Science and Technology, Islamabad for his kind, friendly, encouraging and enthusiastic attitude which gave me courage of facing ups and downs of the process. I have enjoyed every moment of insightful discussion with him, also thanks to **Dr. Rashid Ali**, Assistant Professor, Capital University of Science and Technology, Islamabad.

Without any exaggeration again, I am extremely indebted to **Mr. Khalid Mehmood** and **Mr. Sajid Shah**, the PhD scholars of this department for their ever friendly behavior, inspiring guidance and untiring help during the research period.

My forever thanks goes to all research scholars, friends and colleagues in Mathematics lab for their friendship, help and providing a stimulating and encouraging environment. I wish to show my deep gratitude to my friends **Ayesha**, **Dania Malik**, **Urwa**, **Asma Khan** and **M. Yameen** for their love, personal interest and moral support.

At this juncture, I pay my deep regards to my beloved parents and specially my brothers and sisters **Mr. Mubashar Ashraf**, **Mr. Mudassir Ashraf**, **Mr. Hamid Ashraf**, **Rabia Naheed** and **Fouzia Ashraf** for their selfless care, love, devotion and prayers that made me able to achieve this goal. May Allah bless them all.

Asifa Ashraf

Contents

List of Figures

List of Tables

Abbreviations

PDEs	**P**artial **D**ifferential **E**quations
MHD	**M**agnetohydrodynamics
FEM	**F**inite **E**lement **M**ethod

Nomenclature

ρ	fluid density (kg/m^3)
B_0	magnetic field strength
c_p	specific heat ($Jkg^{-1}k^{-1}$)
k	thermal conductivity (W/m^2K)
Nu_x	local Nusselt number
Nu_{avg}	averaged Nusselt number
Pr	Prandtl number (ν_f/μ_f)
Gr	Grashof number ($g\beta_f(T_h - T_c)H^3/\nu_f^2$)
Ha	Hartmann number ($B_0 H\sqrt{\sigma_{nf}/\rho_{nf}\nu_f}$)
Re	Reynolds number ($u_0 H/\nu_f$)
T	temperature
H	step size (m)
$\mathbf{n}$	unit normal vector
p	pressure (Pa)
P	non-dimensional pressure
q	internal heat generation/absorption parameter
Greek symbols	
α	thermal diffusivity
β	expansion coefficient
γ	inclination angle
θ	non-dimensional temperature
ν	kinematic viscosity
σ	electrical conductivity
ϕ	solid volume fraction
μ	dynamic viscosity

u	velocity component in x ?direction
v	velocity component in y ?direction
U, V	dimensionless velocity components
x	horizontal co-ordinate
y	vertical co-ordinate
X, Y	dimensionless coordinates

Subscripts

c	cold
h	hot
m	average
nf	nanofluid
nd	nondimensional
p	solid particles

Dedicated to ones who gave me life and grew me up
Those angels who were always my supportive.
I owe them each moments of my life and praise
them in every breath.
Dedicated to the most holy person, Mother
NASEEM AKHTAR
And the dearest person, Father
M. ASHRAF SABIR.

Chapter 1

Introduction

Backward facing step flow has long been studied and gained considerable attention in various fields of engineering with applications such as electronic devices, airfoil, combustor and collector of power system [1]. Moreover, mixed convective nanofluid flow and heat transfer attract the interest for its significance and wide practical applications in science and engineering. Mixed convection is one of the mode of the heat transfer that occurs when natural convection and forced convection mechanism act together to transfer heat. It can also be defined as the process where both pressure forces and buoyancy forces interact. Most of the time, it has been seen in very high power output device that the forced convection is not enough to dissipate all of the heat necessary. At this moment, combining natural convection with forced convection would provide the required results. Nuclear technology and few aspects of electronic cooling are the examples of these processes.

Mulaweh [2] investigated the laminar mixed convection flow over backward and forward facing step and presented the effect of various parameters, e.g., Reynolds number, angle of inclination, Prandtl number, ratio expansion, buoyancy force on the flow and temperature difference between the free stream and the heated wall. It was observed that the local Nusselt number decreases with an increase in buoyancy opposing force in the laminar non circulating flow downstream of the step while the reverse trend was observed for recirculating flow region. The effect of buoyancy-assisting force on reattachment length downstream of the step was also observed in this paper. Brkley *at al.* [3] observed the linear stability of backward facing step flow for Reynolds number between 450 - 1050. The results show that up to a Reynolds number of 1050, the two dimensional flow over the backward facing step is linearly stable. The velocity distribution and reattachment length with the help of Laser-Dopplar measurements for downstream of backward facing step was investigated by Armaly *at al.* [4]. He conducted the result for laminar, transitional and turbulent flow of air in Reynolds number between 70 and 8000.

In heat transfer process, nano-sized particles are added in base fluid to obtain better thermal properties. A nanofluid is a fluid containing nanometer-sized particles called nanoparticles. Common base fluids are water, oil, ethylene glycol etc. Nanofluid improve the heat transfer rate of the base fluid. Many researchers conducted the study of nanofluid over backward facing step. Nada [5] numerically investigated the heat transfer over the backward facing step using different types of nanofluid. It was noticed that the nanoparticles having high thermal conductivity outside the recirculation zones have more enhancement on Nusselt number. However, within recirculation zone, nanoparticles having low thermal conductivity have better enhancement on heat transfer. The increase in volume fraction of nanoparticles causes the increase in average Nusselt number. The similar is carried out by many researchers [6, 7]. Kherbeet *at al.* [8] have made numerical investigation of the laminar mixed convection over micro-scale backward facing step with nanofluid for three dimensions. Different types of nanoparticle including Al_2O_3, CuO, SiO_2 and ZnO were used. Their diameter ranges from 25 nm to 70 nm. The Reynolds number used were given the values from the interval [50, 175]. It was noticed that the heat transfer increases with the increase of volume fraction and Reynolds number. The results show that the nanofluid having SiO_2 nanoparticles has maximum heat transfer value. It was observed that the heat transfer rate increases by decreasing the diameter of nanoparticles.

Aswadi *at al.* [9] numerically investigated the laminar flow of forced convection of nanofluid over backward facing step using finite volume method where Reynolds number used were given the values from the interval [50, 175]. When Reynolds number increases, the reattachment point is found to move downstream far from the step. It is noticed that nanofluid of SiO_2 nanoparticles has highest velocity as compared to the other nanofluids while nanofluid having Au nanoparticles has the lowest velocity. Oztop and Selimefendigil [10] investigated the mixed convection heat transfer characteristics for lid-driven cavity within square enclosure heated by corner heaters. It was found that, by increasing the Hartmann number, the heat transfer rate decreases. Pirmohamdi and Ghassemi [11] have studied the steady, laminar, natural convection flow with magnetic field on heat transfer inside a tilted square enclosure. He found that when the Hartmann number increases, the convective heat transfer reduces. Moreover, it was found that value of Nusselt number depends strongly upon the inclination angles for the relatively small value of Hartman number and Nusselt number increases when ϕ increases upto 45°.

The study of behavior of electrical conducting fluid in the presence of electromagnetic field is called magnetohydrodynamics (MHD). It is an important scientific branch and many researchers have done a lot of work on it. In many industrial applications such as liquid metals,

geothermal energy extraction, plasma, purification of molten metals from non-metallic inclusions and in many other applications, magnetohydrodynamics (MHD) flow of an electrically conducting fluid with the heat transfer can be observed. Abbasi and Nassrallah [12] studied the MHD laminar flow of viscous incompressible fluid for a backward facing step and performed the numerical simulations for Reynolds number less than 380 with Prandtl number 0.02 while taking Stuart number from 0 to 0.2. It was found that the heat transfer is significantly enhanced by the magnetic field in the case of high Prandtl number. Mehrez *at al.* [13] studied the effect of magnetic field on mixed convection of Cu-water nanofluid. The governing parameters involved were the Reynolds number, Hartmann number, Richardson number, magnetic field inclination and volume fraction of nanoparticle. It was observed that heat transfer exchange increases by increasing the nanoparticles volume fraction.

Zheng *at al.* [14] numerically studied the two-dimensional mixed convection in a lid-driven cavity with circular cylinder. They used the Immersed-boundary method which is based on the finite volume method. It was found that when the Richardson numbers is 10 with Reynolds number 100, the effect of cylinder position in the cavity on Nusselt number distribution was not strong. It was also observed that when the Richardson number decreases to 0.4 and 0.1 by increasing the Reynolds number up to 500 and 1000, the effect of cylinder position in cavity on the Nusselt number distribution becomes significant. Saha *at al.* [15] investigated the mixed convection flow and heat transfer in lid-driven cavity with wavy bottom surface. The mathematical model was solved by using Galerkin weighted residual method of finite element formulation. The effect of different parameters, e.g., Reynolds number, Grashof number and number of undulation on heat transfer and flow structure was observed. It was found that the heat transfer and flow characteristics inside the cavity were strongly dependent on the number of undulation, Grashof number and Reynolds number.

Heat transfer and mixed convection play an important role in science and engineering fields. In recent years, technology of nanofluid has emerged as a new enhanced heat transfer application. Traditional fluids which were being used for the heat transfer application such as mineral oil, water and ethylene glycol have rather low thermal conductivity. Nanofluid with relatively higher thermal conductivity gained huge interest for researchers due to high potential in heat transfer. Different cases are discussed containing the fluid with nanoparticles such as TiO_2, Cu and Al_2O_3 in various irregular shaped geometries. It is compulsory to study the average Nusselt number for a wavy surface because irregular or wavy surface is often encountered in various applications, e.g., cooling system of micro devices, electrical machinery and many geophysical applications. Moreover, after studying the different induction of copper nanoparticles in fluid flow inside the geometry with inclined cavity shows the enhancement of heat transfer rate with increment in the solid volume fraction ϕ. A similar interest is newly established in recent few decades where heat transfer exchange is studied

with internal heat generation/absorption applied on different models. Different implementations of convective heat transfer of nanofluids using internal heat generation or absorption have been investigated in the last few decades.

Nasrin *at al.* [16] presented the numerical structure of mixed convection heat transfer in lid driven cavity filled with Cu-water nanofluid with internal heat generation. They considered the value of the heat generation parameter in the range 0 - 20 and the effect of pertinent parameters, e.g., solid volume fraction, Richardson number and magnetic field inclination on the flow and heat transfer are presented. The induced results show that Ri plays a dominant role on the heat transfer exchange and an increase in solid volume fraction depicts a dominant impact on the flow pattern. They concluded that by increasing the heat generation parameter, the average Nusselt number decreases. Pavithra and Gireesha [17] investigated the boundary layer flow and heat transfer of dusty fluid over an exponentially stretching surface in the presence of viscous dissipation and internal heat generation/absrption. His study clearly show that temperature in the case of heat source (i.e. generation) is higher than that in the case of sink parameter (absorption). Extension to that, Hamad and Pop [18] theoretically studied the steady boundary layer flow near the stagnation point on a permeable stretching sheet in porous medium saturated with nanofluid in the presence of internal heat generation or absorption. The nanofluid model proposed by Tiwari and Das [19] is used and very successfully applied by many researchers.

Natural convection cooling of a localized heat source at the bottom of nanofluid filled enclosure was analyzed by Ghasemi and Aminossadati [20]. A similar study has been carried out by many researchers. Ogut [21] studied the natural convection of water based nanofluid in inclined enclosures with the heat transfer using the expression for calculating the effect of thermal conductivity of solid liquids mixture. Samad and Mohebujjaman [22] worked on heat and mass transfer for free convective flow along the vertical stretching sheets in the presence of magnetic field with heat generation. Again, Elbashbeshy and Aldawody [23] investigated the unsteady stretching surface involved in porous medium with heat flux variable in the contribution of sink and heat source.

1.1 Thesis Contributions

The aim of this thesis is to examine the mixed convective nanofluid flow over backward facing step for various inclination angle of magnetic field occupied with Cu-water nanoparticles with the contribution of internal heat generation/absorption. The governing equations are solved by using the Galerkin finite element method. The streamlines and isotherms are formed, heat transfer characteristics is obtained for an inclination angle of magnetic field ranging

from 0° to 90°. The effect of Reynolds number, Hartman number, inclination of magnetic field, solid volume fraction and heat generation parameter on the temperature and velocity field are shown graphically and analyzed in detail.

1.2 Thesis outline

We divided this thesis into five chapters.

The brief introduction of the present work is given in **Chapter 1**.

Method of solution of the problem and basic definitions are presented in **Chapter 2**.

Numerical study of mixed convection of nanofluid flow over backward facing step under different inclination angle of magnetic field is presented in **Chapter 3**.

The effect of internal heat generation/absorption on mixed convective nanofluid flow is dealt in **Chapter 4**.

Conclusion of the present work is summarized in **Chapter 5**.

Chapter 2

Fundamental Concepts and Governing Equations

2.1 Some basic definitions

Definition 2.1.1. (Fluid)

Fluid is a substance that deforms continuously under the influence of shear stress applied on it. It has zero shear force applied to it. It changes its shape at a steady rate when acted upon by a force.

Definition 2.1.2. (Fluid mechanics)

Fluid mechanics is the branch of physics that deals with the study of laws of force and properties of fluid and the effect of forces on it. It is divided into two branches, i.e., fluid dynamics and fluid statics.

Definition 2.1.3. (Fluid dynamics)

Fluid dynamic is the branch of fluid mechanics which deals with the study of fluids in motion.

Definition 2.1.4. (Fluid statics)

Fluid statics is the branch of fluid mechanics which deals with the study of fluids at rest.

Definition 2.1.5. (Pressure)

The amount of applied force per unit area is called pressure. It is denoted by P and mathematically, it can be written as

$$P = \frac{F}{A}, \tag{2.1}$$

where F and A denote the applied force and area of the surface, respectively.

Definition 2.1.6. (Density)

It is defined as the mass per unit volume. The dimension of density is $[ML^{-3}]$ and its unit is kg/m^3. It is denoted by ρ and mathematically, it can be written as

$$\rho = \frac{m}{V}, \tag{2.2}$$

where m and V are the mass and volume of the material, respectively.

Definition 2.1.7. (Stress)

Stress is defined as the force per unit area within the distortable body. Mathematically, it can be written as

$$\rho = \frac{F}{A}, \tag{2.3}$$

where F shows the force and A represents area. There are normal stresses and tangential stresses.

Definition 2.1.8. (Normal stress)

Normal stress is the component of stress in which a force act normal to the unit surface area.

Definition 2.1.9. (Tangential stress)

In tangential stress, force acts parallel to the unit surface area, e.g., shear stress.

Definition 2.1.10. (Viscosity)

The extent which measures the resistance of fluid tending to cause the fluid to flow is called viscosity. It is denoted by μ and mathematically, it can be expressed by

$$\mu = \frac{\text{shear stress}}{\text{shear strain}}.$$

Definition 2.1.11. (Kinematic viscosity)

Kinematic viscosity is the ratio between the dynamic density and viscosity. Symbolically, it can be written as ν and mathematically, it is expressed by

$$\nu = \frac{\mu}{\rho}, \tag{2.4}$$

where μ denotes the dynamic viscosity and ρ is the density.

Definition 2.1.12. (Dynamic viscosity)

Dynamic viscosity is the measure of internal resistance. It is denoted by μ and expressed by

$$\mu = \tau \left(\frac{dy}{dc} \right), \tag{2.5}$$

where dy is the unit distance between layers and dc is the unit velocity.

Definition 2.1.13. (Magnetohydrodynamics)

The branch of dynamics which deal with the study of magnetic properties of electrically conducting fluid is called magnetohydrodynamics such as plasma, liquid metal and salt water etc.

2.2 Classification of fluids

Definition 2.2.1. (Ideal fluid)

The fluid which is incompressible and has no viscosity ($\mu = 0$) is called an ideal fluid. It is also called inviscid fluid. There is no existence of shear force because the viscosity is vanishing in an ideal fluid.

$$\tau_{yx} = \mu \left(\frac{du}{dy} \right), \tag{2.6}$$

where τ_{yx} is shear stress.

Definition 2.2.2. (Real fluid)

The fluid which is compressible in nature and has some viscosity is said to be a real or viscous fluid. As the fluid moves, certain amount of resistance is always offered by these fluids.

Definition 2.2.3. (Nanofluid)

The fluid containing nanometer-sized particles is called nanofluid. The nanoparticles are typically made of metals, oxides or carbon nanotubes. Examples of base fluid include water, ethylene glycol etc.

Definition 2.2.4. (Newtonian fluid)

Newtonian fluid is defined as the fluid for which shear stress is directly and linearly proportional to the deformation rate. Newtonian fluids have linear relationship between the shear stress and deformation rate. In other words, the fluids which satisfy the Newton's law of viscosity are called Newtonian fluids. The common examples of such fluids are water, silicon oil and gasoline etc. Shear stress of Newtonian fluid is mathematically defined as

$$\tau_{yx} = \mu \frac{du}{dy}, \tag{2.7}$$

where τ_{yx} is the shear stress, u denotes x-component of velocity and μ denotes dynamic viscosity.

Definition 2.2.5. (Non-Newtonian fluid)

In Non-newtonian fluids, shear stress is not directly proportional to the rate of deformation. In other words, the fluid which does not satisfy the Newton law of viscosity is said to be non newtonian fluid. Examples of Non-newtonian fluid are shampoo, grease, paint, blood and melt polymer etc. Mathematically, it can be written as

$$\tau_{xy} \propto \left(\frac{du}{dy}\right)^m, \ m \neq 1,$$

$$\tau_{xy} = \nu \left(\frac{du}{dy}\right), \ \nu = j \left(\frac{du}{dy}\right)^{m-1}. \tag{2.8}$$

where ν denotes the apparent viscosity, m is the index of flow performance and the constancy index is j.

2.3 Types of Flow

Definition 2.3.1. (Flow) An object exhibits the flow if unlike forces lead to an unbounded distortion. Different types of flow are given as follows:

Definition 2.3.2. (Laminar flow)

The flow in which streamlines are parallel to each other is said to be laminar. Smoke rising is the example of laminar flow. If we observe the smoke rising from cigarette, for the first few seconds the flow is laminar but after few second, it becomes turbulent.

Definition 2.3.3. (Turbulent flow)

The flow in which streamlines intersect each other is said to be turbulent. This type of flow cannot be handled easily.

Definition 2.3.4. (Uniform flow)

If the velocity of the flow has the same direction as well as magnitude during the motion of fluid, then it is called uniform flow. Mathematically, it can be written as

$$\frac{\partial \mathbf{V}}{\partial s} = 0, \tag{2.9}$$

where $\mathbf{V}$ is the velocity and s is the displacement in any direction.

Definition 2.3.5. (Non uniform flow)

If the velocity is not same at every point in the fluid at a given instant, then it is said to be non uniform flow. It may be steady or unsteady. Mathematically, it is expressed as

$$\frac{\partial \mathbf{V}}{\partial s} \neq 0, \tag{2.10}$$

where $\mathbf{V}$ is the velocity and s is the displacement.

Definition 2.3.6. (External flow)

The flow which is not bounded by the solid surface is called external flow. The flow of water in the ocean or in the river is the example of the external flow.

Definition 2.3.7. (Internal flow)

The flow which is bounded by the solid surface is called internal flow. The example of such flow is the flow in the glass or in a pipe .

Definition 2.3.8. (Steady flow)

The flow having no change with time is said to be steady flow.
Mathematically, it can be written as

$$\frac{d\eta^*}{dt} = 0, \tag{2.11}$$

where η^* is fluid property.

Definition 2.3.9. (Unsteady flow)

The flow having change with time is known as unsteady flow. Mathematically, it can be written as

$$\frac{d\eta^*}{dt} \neq 0, \tag{2.12}$$

where η^* is fluid property.

Definition 2.3.10. (Compressible flow)

The flow in which the density with respect to the substance variable varies during the flow is said to be compressible flow. Mathematically, it is expressed by

$$\rho(x, y, z, t) \neq c, \tag{2.13}$$

where 'c' is a constant.

Definition 2.3.11. (Incompressible flow)

The flow in which the density remains same throughout during the flow is called incompressible flow. Mathematically, it can be written as

$$\rho(x, y, z, t) = c, \tag{2.14}$$

where 'c' is a constant.

2.4 Heat transfer Mechanism

There are three types of heat transfer

Definition 2.4.1. (Conduction)

The flow of heat through solid or liquid by the intersection of free electrons and molecules is said to be conduction. In other words, the heat is transfered between those objects that are

in physical constant is called conduction. Mathematically, it can be written as

$$q = -kA\left(\frac{\Delta T}{\Delta n}\right), \tag{2.15}$$

where k denotes the constant of the thermal conductivity and $\frac{\Delta T}{\Delta n}$ denote the gradient of the temperature respectively.

Definition 2.4.2. (Convection)

A process in which heat transfer occurs due to the movement of group of molecules within the fluid. Gases and liquids are the examples of convection fluid. It takes place through diffusion or advection. Mathematically, it is expressed as

$$q = hA(T_s - T_\infty), \tag{2.16}$$

where h, A, T_s and T_∞ denote the heat transfer coefficient, the area, the temperatures of the surfaces and the temperatures away from the surfaces, respectively. It is subdivided into the following three categories.

Definition 2.4.3. (Force convection)

A method of heat transfer in which motion of fluid is obtained by an independent sources, i.e., a pump or fan is called force convection.

Definition 2.4.4. (Natural convection)

A method in which fluid motion is not generated by an independent source, it is said to be natural convection. It is also called free convection. In other words, it exists due to the temperature difference which affects the buoyancy and density of the fluids. Natural convection occurs only when there is a gravitational field.

Definition 2.4.5. (Mixed convection)

A method in which both forced and natural convection processes simultaneously and significantly involve in the heat transfer is called mixed convection.

Definition 2.4.6. (Radiation)

When two bodies at different temperatures are aligned then radiation effect is occurred. In the liquid and gases, the radiation and convection play a major role by transferring heat

but in solids radiation is usually negligible and convection is totally absent. Thus for solid substances, conduction plays a major role in heat transfer. For example, under the sun rays if we place a material object, e.g. a piece of steel, after a few moments we observe that the material object is heated. Such phenomena takes place due to radiation. Mathematically, it can be written as

$$q = E\sigma A[(\Delta T)^4], \tag{2.17}$$

where E, σ, $(\Delta T)^4$, A, q are the emissivity of the scheme, the constant of Stephan-Boltzmann ($5.670 \times 10^{-}8\frac{W}{m^2K^4}$), the area and the heat transfer, the variation of the temperature respectively.

Definition 2.4.7. (Joule heating)

With finite conductivity when a current flows through a solid or liquid, through resistive loses in the substance, electric energy is transformed to heat energy. Through collisions when conduction electrons shift energy to the conductor's atom then heat is produced on the micro scale, micro valves, cooking plates and toasters applications depend on the Joule heating.

Definition 2.4.8. (Thermal conductivity)

The property of a material related to its capacity to conduct heat is known as thermal conductivity. Fouriers law of conduction which relates the rate of heat transfer by conduction to the temperature gradient is

$$\frac{dQ}{dt} = -kA\frac{dT}{dx}, \tag{2.18}$$

where A, k, $\frac{dQ}{dt}$, $\frac{dT}{dx}$ are the area, the thermal conductivity, the rate of heat transfer and the temperature gradient respectively. With the increase of temperature, thermal conductivity of the most of the liquids decreases except water. The SI unit of thermal conductivity is $\frac{Kg.m}{s^3}$ and its dimension is $[\frac{ML}{T^3}]$.

Definition 2.4.9. (Thermal diffusivity)

Thermal diffusivity is material's property for characterizing unsteady heat conduction (k) of a substance to the product of specific heat at constant pressure (c_p) and density (ρ). It measures the ability of a substance to transfer thermal energy relative to its ability to store. Mathematically, it can be written as

$$\alpha = \frac{k}{\rho c_p}. \tag{2.19}$$

2.5 Dimensionless numbers

Definition 2.5.1. (Prandtl number)

The ratio of the kinematic diffusivity or momentum diffusivity to the thermal diffusivity is said to be the Prandtl number. It is denoted by Pr and mathematically it can be written as

$$Pr = \frac{\upsilon}{\alpha} = \frac{\frac{\mu}{\rho}}{\frac{k}{\rho c_p}} = \frac{\mu c_p}{k}, \tag{2.20}$$

where ν and α denote the momentum diffusivity or kinematic diffusivity and the thermal diffusivity, respectively. It controls the relative thickness of momentum and temperature function. Physical aspect of Prandtl number gives the respective thickness of thermal boundary layer and velocity boundary layer. For smaller Pr, heat declines quickly as compared to momentum.

Definition 2.5.2. (Grashof number)

The relationship between viscous force and buoyancy force that are acting on a fluid is called Grashof number. It repeatedly occurs in the situation relating free convection. Symbolically it is denoted by Gr and mathematically, it can be written as

$$Gr = \frac{g\beta_f(T_h - T_c)H^3}{\nu_f^2}, \tag{2.21}$$

where, β_f, g, T_h, T_c, H, ν denote the coefficient of the expansion, the gravitational acceleration, the hot temperature, the cold temperature, the step size and the kinematic viscosity, respectively.

Definition 2.5.3. (Hartmann number)

The ratio of electromagnetic force to the viscous force is called Hartmann number. It was first introduced by Hartmann. It is denoted by Ha.

Definition 2.5.4. (Reynolds number)

Reynolds number for the fluid behavior in the boundary layer is specified as the relationship of inertial forces to the viscous forces. Inertial forces act upon all masses in a non-inertial frame of reference while viscous forces are the internal fluid flow resistance. It is denoted by

Re and mathematically it can be written as

$$Re = \frac{\mu_o H}{\nu_f}, \tag{2.22}$$

where μ_o denotes the dynamic velocity, H denotes the step size and ν_f represents the kinematic viscosity of fluid. Turbulent flow occurs at high Reynolds number due to the dominance of inertial force while for a low Reynolds number, laminar flow arises where viscous forces are dominant which is characterized by the laminar flow.

Definition 2.5.5. (Nusselt number)

It is the relationship between convective to the conductive heat transfer through the boundary of the surface. It was first introduced by the German mathematician Nusselt and is denoted by Nu. Mathematically, local Nusselt number of nanofluid is calculated as

$$Nu_x = -\frac{k_{nf}}{k_f}\left(\frac{\partial \theta}{\partial n}\right), \tag{2.23}$$

where k, θ and n denote the thermal conductivity , dimensionless temperature and surface normal direction, respectively.
Average Nusselt number is achieved by integrating the local Nusselt number as

$$Nu_{avg} = \int Nu_x \, dx. \tag{2.24}$$

Definition 2.5.6. (Richardson number)

The intensity of the buoyancy term to the flow shear term is called Richardson number. It is introduced by Lewis Fry Richardson. The Richardson number can be expressed by using a combination of the Reynolds number and Grashof number given as

$$Ri = \frac{Gr}{Re^2}. \tag{2.25}$$

2.6 Basic equations

Definition 2.6.1. (Continuity equation)

The law of conservation of mass states that mass in a classical system is conserved. It is derived from the law of conservation of mass and mathematically, it is expressed by

$$\frac{\partial \rho}{\partial t} + \nabla.(\rho \mathbf{V}) = \mathbf{0}, \tag{2.26}$$

where t is the time.
For incompressible fluid, continuity equation takes the form

$$\nabla.\mathbf{V} = \mathbf{0}. \tag{2.27}$$

Definition 2.6.2. (Law of conservation of momentum)

Each particle of fluids which is in state of steady or accelerated motion obey Newton second law of motions. This law illustrates that the combination of applied external force working on a scheme is equal to times rate of changes of linear momentums of the scheme. This law is expressed as

$$\rho\frac{d\mathbf{V}}{dt} = \text{div}\tau + \rho b, \tag{2.28}$$

For Navier-Stokes equation

$$\tau = -pI + \mu A_1, \tag{2.29}$$

where A_1 is the tensor and first time it was produced by Rivlin-Erickson.

$$A_1 = \text{grad}\mathbf{V} + (\text{grad}\mathbf{V})^t, \tag{2.30}$$

In the above, $\frac{d}{dt}$ denotes material time derivative or total derivative, ρ denotes density, $\mathbf{V}$ denotes velocity field, τ is the Cauchy stress tensor, b is the body forces, p is the pressure and μ denotes the dynamic viscosity.
The matrix form of Cauchy stress tensor is expressed by

$$T = \begin{pmatrix} \sigma_{xx} & \tau_{yx} & \tau_{zx} \\ \tau_{xy} & \sigma_{yy} & \tau_{zy} \\ \tau_{xz} & \tau_{yz} & \sigma_{zz} \end{pmatrix}, \tag{2.31}$$

where σ_{xx}, σ_{yy} and σ_{zz} are normal stresses, otherwise the shear stresses. For two-dimensional flow, we have $\mathbf{V} = [u(x, y, 0), v(x, y, 0), 0]$ and thus

$$\text{grad}\mathbf{V} = \begin{pmatrix} \frac{\partial u}{\partial x} & \frac{\partial u}{\partial y} & 0 \\ \frac{\partial v}{\partial x} & \frac{\partial v}{\partial y} & 0 \\ 0 & 0 & 0 \end{pmatrix}. \tag{2.32}$$

Substituting Eq. (2.31) and (2.32) in Eq. (2.29), we obtain

$$\frac{\partial u}{\partial t} + u\frac{\partial u}{\partial x} + v\frac{\partial v}{\partial y} = -\frac{1}{\rho}\frac{\partial p}{\partial y} + \nu\left(\frac{\partial^2 u}{\partial x^2} + \frac{\partial^2 u}{\partial y^2}\right). \tag{2.33}$$

Similarly, by repeating the above process for V component, we get

$$\frac{\partial v}{\partial t} + u\frac{\partial v}{\partial x} + v\frac{\partial v}{\partial y} = -\frac{1}{\rho}\frac{\partial p}{\partial y} + \nu\left(\frac{\partial^2 v}{\partial x^2} + \frac{\partial^2 v}{\partial y^2}\right). \tag{2.34}$$

2.6.1 Energy equation

The energy equation is

$$\rho c_p\left(\frac{\partial}{\partial t} + \mathbf{V}.\nabla\right)T = k\nabla^2 T + \tau L + \rho c_p\left[D_B\nabla C.\nabla T + \frac{DT}{Tm}\nabla T\right], \tag{2.35}$$

where $(c_p)_f$ denotes the specific heat of the basic fluid, $(c_p)_s$ is the specific heat of the material, ρ_f is the density of basic fluid, L denotes the rate of strain tensor and T is the temperature of the fluid, D_B represents the Brownian motion coefficient D_T denotes the temperature diffusion coefficient and T_m denotes the mean temperature. The expression for Cauchy stress tensor τ for viscous incompressible fluid is expressed by

$$\tau = -pI + \mu A_1, \tag{2.36}$$

$$A_1 = \text{grad}\mathbf{V} + (\text{grad}\mathbf{V})^t, \tag{2.37}$$

where t represents transpose of the matrix for two dimensional field velocity of the fluid, T the stain tensor and can be written as

$$T = \begin{pmatrix} \sigma_{xx} & \tau_{yx} & \tau_{zx} \\ \tau_{xy} & \sigma_{yy} & \tau_{zy} \\ \tau_{xz} & \tau_{yz} & \sigma_{zz} \end{pmatrix}. \tag{2.38}$$

2.7 Finite Element Method

The finite element method is a numerical scheme for finding the approximate solution of boundary value problem for partial differential equations. Finite element method subdivides a huge problem into smaller parts, named as the finite elements. A finite element method is simulated by a weak formulation, one or more solution algorithms and post processing procedure. Examples of weak formulation are the weighted residual method, the discontinuous Galerkin method, mixed method, etc. [24]

Definition 2.7.1. (Galerkin Finite Element Method)

The area of numerical analysis in which Galerkin method is the class of method for converting the continuous problems into discrete problems. Principally, it is similar to variational method for applying parameters to the functional space, by interchanging the equations to the weak formulation [25]. It contains the following steps

1. Multiply both sides of governing equations of the problem by test function w ϵ W, that is vanishing on the boundaries of the domain, where W is a test space.
2. Perform integration by parts such that some derivatives will be transferred from trial to test function.
3. Include natural boundary conditions in boundary integrals and build essential boundary conditions into trial space U and test space W. This is called variational formulation.
4. Generate triangulation or mesh. Divide the entire domain into non-overlapping elements. In one dimension, mesh is a set of points that is, $x_0 = 0, x_1, x_2, ...x_N = 1$, where x_i is called a node and $e_i = \{x_i, x_{i+1}\}$ is an element such that $e_i \bigcap e_j = \varphi$ for $i \neq j$. $h_i = x_i - x_{i-1}$ for $i = 0, 1, ...N$ is called mesh size.
5. Approximate the infinite dimensional trial space U and test space W by finite dimensional spaces U_h, V_h and W_h, respectively where U_h (finite dimensional space) $\subset U$ (solution space).
6. Choose the basis functions φ_1,φ_2,...φ_N of w_h, so that every test function $w_h \epsilon\ W_h$ can be written as $w_h = \sum w_i \varphi_i \epsilon\ W_h$ for $i = 1, ...N$.
7. Find $u_h \epsilon U_h$ such that $a(u_h, w_h) = b(w_h)\ \forall\ w_h = \sum w_i \varphi_i\ \epsilon W_h$ for $i = 1, ...N$,
   $\Rightarrow a(u_h, \varphi_i) = b(\varphi_i)$, where $i = 1, ..., N$.
   Substituting $u_h = \sum u_j \varphi_j$, for $j = 1, ...N$,
   $a(\sum u_j \varphi_j, \varphi_i) = b(\varphi_i)$ for i, $j = 1, 2, 3..., N$,
   $\Rightarrow \sum a(\varphi_j, \varphi_i) u_j = b(\varphi_i)$ for i, $j = 1, 2, 3..., N$.
   where u_j are the solution values at the nodes. Also $a(u, w)$ is bilinear form and $b(w)$ is the linear form.

2.7.1 Advantages

- Finite element method is very good in managing complex geometrical boundaries [24].
- There are many commercial packages based on finite element method, i.e., ADINA, ANSYS for analyzing practical problems [25].

Chapter 3

Influence of magnetic field inclination on mixed convective flow over backward facing step

In this chapter, we perform the numerical study of laminar mixed convection of nanofluid flow over a backward facing step under the influence of inclination angles of magnetic field. By using an appropriate transformation, we transform the system of nonlinear dimensional partial differential equations into coupled dimensionless partial differential equations. Finite element technique together with Galerkin weighted residual method has been used to solve the considered problem. The impact of governing parameters is analyzed through streamlines and isotherms. In this chapter, review of the research paper [26] has been presented.

3.1 Problem Formulation

Let us consider the laminar, two-dimensional, steady incompressible viscous flow of an electrically conducting fluid in backward facing step filled with Cu-water nanofluid. Schematic diagram of the system under investigation is shown in the Figure 3.1. The size of backward facing step is H and channel height is given as $2H$. The inflow side of the channel, constant velocity and uniform temperature T_c are considered. The bottom wall of the channel downstream of the step is isothermally heated while the other walls are assumed to be adiabatic with no-slip boundary conditions. The thermophysical properties of the fluid [26] are shown in Table 3.1. Under these assumptions, the governing equations of continuity, momentum and energy [23] which model the flow can be expressed in dimensional form given as .

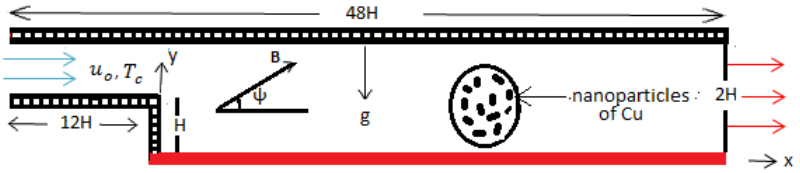

FIGURE 3.1: Geometry of the physical model.

Property	Water	Copper
ρ	997.1	8954
c_p	4179	383
k	0.6	400
β	2.1×10^{-4}	1.67×10^{-5}
σ	0.05	5.97×10^{7}

TABLE 3.1: Thermophysical properties of water and copper [26].

Continuity equation:

$$\frac{\partial u}{\partial x} + \frac{\partial v}{\partial y} = 0, \tag{3.1}$$

Momentum equation for u-velocity:

$$u\frac{\partial u}{\partial x} + v\frac{\partial u}{\partial y} = -\frac{1}{\rho_{nf}}\frac{\partial p}{\partial x} + \nu_{nf}\left(\frac{\partial^2 u}{\partial x^2} + \frac{\partial^2 u}{\partial y^2}\right) + \frac{\sigma_{nf}B_0^2}{\rho_{nf}}\left(v\sin(\psi)\cos(\psi) - u\sin^2(\psi)\right), \tag{3.2}$$

Momentum equation for v-velocity:

$$u\frac{\partial v}{\partial x} + v\frac{\partial v}{\partial y} = -\frac{1}{\rho_{nf}}\frac{\partial p}{\partial y} + \nu_{nf}\left(\frac{\partial^2 v}{\partial x^2} + \frac{\partial^2 v}{\partial y^2}\right) + \frac{\sigma_{nf}B_0^2}{\rho_{nf}}\left(u\sin(\psi)\cos(\psi) - v\cos^2(\psi)\right) + \beta_{nf}g(T - T_c), \tag{3.3}$$

Energy equation:

$$u\frac{\partial T}{\partial x} + v\frac{\partial T}{\partial y} = \alpha_{nf}\left(\frac{\partial^2 T}{\partial x^2} + \frac{\partial^2 T}{\partial y^2}\right). \tag{3.4}$$

Here u, v denote the velocity components, the kinematic fluid velocity is ν, the fluid density is ρ, the specific heat is c_p, the fluid thermal conductivity is k, the magnetic field strength is B_0, the electrical conductivity is σ, the expansion coefficient is β, ψ is the inclination angle of magnetic field and α is the thermal diffusivity of the nanofluid.

Nanofluid properties	Expressed model
Density	$\rho_{nf} = (1\text{-}\phi)\rho_f + \phi\rho_p$
Specific heat	$(\rho c_p)_{nf} = (1\text{-}\phi)(\rho c_p)_f + \phi(\rho c_p)_p$
Thermal diffusivity	$\alpha_{nf} = k_{nf}/(\rho c_p)_{nf}$
Electrical conductivity	$\sigma_{nf} = (1\text{-}\phi)\sigma_f + \phi\sigma_p$
Thermal expansion coefficient	$(\rho\beta)_{nf} = (1\text{-}\phi)(\rho\beta)_f + \phi(\rho\beta)_p$

TABLE 3.2: Implemented formulas for the nanofluid properties [23].

3.2 Non-dimensional Form of the Governing Equations

By using the following dimensionless parameters [20], Eqs. (3.1) - (3.4) are converted into the dimensionless form as follows

$$Gr = \frac{g\beta_f(T_h - T_c)H^3}{\nu_f^2}, \qquad Pr = \frac{\nu_f}{\alpha_f}, \qquad Re = \frac{u_0 H}{\nu_f}, \qquad Ri = \frac{Gr}{Re^2}, \qquad Ha = B_0 H\sqrt{\frac{\sigma_f}{\mu_f}}.$$

Dimensionless variables involved are

$$X = \frac{x}{H}, \qquad Y = \frac{y}{H}, \qquad U = \frac{u}{u_0}, \qquad V = \frac{v}{u_0}, \qquad P = \frac{p}{\rho_f u_0^2}, \qquad \theta = \frac{T - T_c}{T_h - T_c}.$$

The governing dimensionless equations are given by

$$\frac{\partial U}{\partial X} + \frac{\partial V}{\partial Y} = 0, \tag{3.5}$$

$$U\frac{\partial U}{\partial X} + V\frac{\partial U}{\partial Y} = -\frac{\partial P}{\partial X} + \frac{1}{Re}\frac{\rho_f}{\rho_{nf}}\frac{1}{(1-\phi)^{2.5}}\left(\frac{\partial^2 U}{\partial X^2} + \frac{\partial^2 U}{\partial Y^2}\right) + \frac{\rho_f}{\rho_{nf}}\frac{\sigma_{nf}}{\sigma_f}\frac{Ha^2}{Re}\left(V\sin(\psi)\cos(\psi) - U\sin^2(\psi)\right), \tag{3.6}$$

$$U\frac{\partial V}{\partial X} + V\frac{\partial V}{\partial Y} = -\frac{\partial P}{\partial Y} + \frac{1}{Re}\frac{\rho_f}{\rho_{nf}}\frac{1}{(1-\phi)^{2.5}}\left(\frac{\partial^2 V}{\partial X^2} + \frac{\partial^2 V}{\partial Y^2}\right) + Ri\frac{\rho_f}{\rho_{nf}}\left(1 - \phi + \frac{\rho_s\beta_s}{\rho_f\beta_f}\phi\right)\theta + \frac{\rho_f}{\rho_{nf}}\frac{\sigma_{nf}}{\sigma_f}\frac{Ha^2}{Re}\left(U\sin(\psi)\cos(\psi) - V\cos^2(\psi)\right), \tag{3.7}$$

$$U\frac{\partial \theta}{\partial X} + V\frac{\partial \theta}{\partial Y} = \frac{\alpha_{nf}}{\alpha_f}\frac{1}{RePr}\left(\frac{\partial^2 \theta}{\partial X^2} + \frac{\partial^2 \theta}{\partial Y^2}\right). \tag{3.8}$$

The non-dimensional boundary condition along the channel wall in appropriate form are given as

- On the inlet of channel:

$$U = 1, \quad V = 0, \quad \theta = 0, \tag{3.9}$$

- On the bottoms wall:

$$U = 0, \quad V = 0, \quad \theta = 1, \tag{3.10}$$

- On the outlet of channel:

$$\frac{\partial U}{\partial X} = 0, \quad V = 0, \quad \frac{\partial \theta}{\partial X} = 0, \tag{3.11}$$

- On the rest of walls of channel:

$$U = 0, \quad V = 0, \quad \frac{\partial \theta}{\partial n} = 0. \tag{3.12}$$

  where n represent the surface normal direction.

Implemented formulas for nanofluid [23] as given in Table 3.2

3.3 Numerical solution

The systems of coupled non-linear partial differential Eqs. (3.5) - (3.8) together with the boundary conditions (3.9) - (3.12) has been solved numerically by finite element method together with the Galerkin weighted residual method. First, we established the weak formulation of the governing equations and then approximated the solution utilizing the Galerkin approximation procedure.

3.3.1 Variational/Weak Formulation

Variational form is an approach in which the governing equations are converted from strong form into weak form by multiplying with test function before they are integrated over the entire domain (Ω).

Strong form:

$$U\frac{\partial U}{\partial X}+V\frac{\partial U}{\partial Y}=-\frac{\partial P}{\partial X}+\frac{1}{Re}\frac{\rho_f}{\rho_{nf}}\frac{1}{(1-\phi)^{2.5}}\left(\frac{\partial^2 U}{\partial X^2}+\frac{\partial^2 U}{\partial Y^2}\right)+\frac{\rho_f}{\rho_{nf}}\frac{\sigma_{nf}}{\sigma_f}\frac{Ha^2}{Re}\left(V\sin(\psi)\cos(\psi)-U\sin^2(\psi)\right), \tag{3.13}$$

$$U\frac{\partial V}{\partial X}+V\frac{\partial V}{\partial Y}=-\frac{\partial P}{\partial Y}+\frac{1}{Re}\frac{\rho_f}{\rho_{nf}}\frac{1}{(1-\phi)^{2.5}}\left(\frac{\partial^2 V}{\partial X^2}+\frac{\partial^2 V}{\partial Y^2}\right)+Ri\frac{\rho_f}{\rho_{nf}}\left(1-\phi+\frac{\rho_s\beta_s}{\rho_f\beta_f}\phi\right)\theta+\frac{\rho_f}{\rho_{nf}}\frac{\sigma_{nf}}{\sigma_f}\frac{Ha^2}{Re}\left(U\sin(\psi)\cos(\psi)-V\cos^2(\psi)\right), \tag{3.14}$$

$$\frac{\partial U}{\partial X}+\frac{\partial V}{\partial Y}=0, \tag{3.15}$$

$$U\frac{\partial \theta}{\partial X}+V\frac{\partial \theta}{\partial Y}=\frac{\alpha_{nf}}{\alpha_f}\frac{1}{RePr}\left(\frac{\partial^2 \theta}{\partial X^2}+\frac{\partial^2 \theta}{\partial Y^2}\right). \tag{3.16}$$

Variational form:

Let W = ($H^1(\Omega)$, $H^1(\Omega)$, $H^1(\Omega)$) be the test space for velocity components and temperature and Q = $L^2(\Omega)$ is the test space for pressure. A variational form is as follows:

Find (U, V, θ, P) ϵ W $\times$ Q such that

$$\int_\Omega\left(U\frac{\partial U}{\partial X}+V\frac{\partial U}{\partial Y}\right)\,w\,d\Omega-\frac{\rho_f}{\rho_{nf}}\frac{\sigma_{nf}}{\sigma_f}\frac{Ha^2}{Re}\int_\Omega\left(V\sin(\psi)\cos(\psi)-U\sin^2(\psi)\right)\,w\,d\Omega-\frac{1}{Re}\frac{\rho_f}{\rho_{nf}}\frac{1}{(1-\phi)^{2.5}}\int_\Omega\left(\frac{\partial^2 U}{\partial X^2}+\frac{\partial^2 U}{\partial Y^2}\right)\,w\,d\Omega+\int_\Omega\frac{\partial P}{\partial X}\,w\,d\Omega=0, \tag{3.17}$$

$$\int_\Omega\left(U\frac{\partial V}{\partial X}+V\frac{\partial V}{\partial Y}\right)\,w\,d\Omega-\frac{1}{Re}\frac{\rho_f}{\rho_{nf}}\frac{1}{(1-\phi)^{2.5}}\int_\Omega\left(\frac{\partial^2 V}{\partial X^2}+\frac{\partial^2 V}{\partial Y^2}\right)\,w\,d\Omega-\frac{\rho_f}{\rho_{nf}}\frac{\sigma_{nf}}{\sigma_f}\frac{Ha^2}{Re}\int_\Omega\left(U\sin(\psi)\cos(\psi)-V\cos^2(\psi)\right)\,w\,d\Omega-Ri\frac{\rho_f}{\rho_{nf}}\left(1-\phi+\frac{\rho_s\beta_s}{\rho_f\beta_f}\phi\right)\int_\Omega\theta\,w\,d\Omega+\int_\Omega\frac{\partial P}{\partial Y}\,w\,d\Omega=0, \tag{3.18}$$

$$\int_\Omega\left(\frac{\partial U}{\partial X}+\frac{\partial V}{\partial Y}\right)\,q\,d\Omega=0, \tag{3.19}$$

$$\int_\Omega\left(U\frac{\partial \theta}{\partial X}+V\frac{\partial \theta}{\partial Y}\right)\,w\,d\Omega-\frac{\alpha_{nf}}{\alpha_f}\frac{1}{RePr}\int_\Omega\left(\frac{\partial^2 \theta}{\partial X^2}+\frac{\partial^2 \theta}{\partial Y^2}\right)\,w\,d\Omega=0. \tag{3.20}$$

for all $(w,\, q)\ \epsilon$ W $\times$ Q.
Let $U \approx U_h$, $V \approx V_h$, $\theta \approx \theta_h$, $P \approx P_h$.
$w \approx w_h$, $q \approx q_h$.

Then the Galerkin finite element method yields the following non-linear equations

$$\frac{1}{Re}\frac{\rho_f}{\rho_{nf}}\frac{1}{(1-\phi)^{2.5}}\int_\Omega\left(\frac{\partial U_h}{\partial X}\frac{\partial w_h}{\partial X}+\frac{\partial U_h}{\partial Y}\frac{\partial w_h}{\partial Y}\right)\,d\Omega+\int_\Omega\left(U_h\frac{\partial U_h}{\partial X}+V_h\frac{\partial U_h}{\partial Y}\right)\,w_h\,d\Omega$$
$$-\frac{\rho_f}{\rho_{nf}}\frac{\sigma_{nf}}{\sigma_f}\frac{Ha^2}{Re}\int_\Omega\left(V_h\sin(\psi)\cos(\psi)-U_h\sin^2(\psi)\right)\,w_h\,d\Omega+\int_\Omega\frac{\partial P_h}{\partial X}\,w_h\,d\Omega=0, \quad (3.21)$$

$$\frac{1}{Re}\frac{\rho_f}{\rho_{nf}}\frac{1}{(1-\phi)^{2.5}}\int_\Omega\left(\frac{\partial V_h}{\partial X}\frac{\partial w_h}{\partial X}+\frac{\partial V_h}{\partial Y}\frac{\partial w_h}{\partial Y}\right)\,d\Omega+\int_\Omega\left(U_h\frac{\partial V_h}{\partial X}+V_h\frac{\partial V_h}{\partial Y}\right)\,w_h\,d\Omega$$
$$-Ri\frac{\rho_f}{\rho_{nf}}\left(1-\phi+\frac{\rho_s\beta_s}{\rho_f\beta_f}\phi\right)\int_\Omega\theta_h\,w_h\,d\Omega$$
$$-\frac{\rho_f}{\rho_{nf}}\frac{\sigma_{nf}}{\sigma_f}\frac{Ha^2}{Re}\int_\Omega\left(U_h\sin(\psi)\cos(\psi)-V_h\cos^2(\psi)\right)\,w_h\,d\Omega+\int_\Omega\frac{\partial P_h}{\partial Y}\,w_h\,d\Omega=0, \quad (3.22)$$

$$\int_\Omega\left(\frac{\partial U_h}{\partial X}+\frac{\partial V_h}{\partial Y}\right)\,q_h\,d\Omega=0, \quad (3.23)$$

$$\frac{\alpha_{nf}}{\alpha_f}\frac{1}{RePr}\int_\Omega\left(\frac{\partial\theta_h}{\partial X}\frac{\partial w_h}{\partial X}+\frac{\partial\theta_h}{\partial Y}\frac{\partial w_h}{\partial Y}\right)\,d\Omega+\int_\Omega\left(U_h\frac{\partial\theta_h}{\partial X}+V_h\frac{\partial\theta_h}{\partial Y}\right)\,w_h\,d\Omega=0. \quad (3.24)$$

Using the FEM approximations of U_h, V_h, P_h and θ_h, the fully discrete block system reads the following

$$\begin{bmatrix} a_{11}L+b_{11}M+N(\underline{U},\underline{V}) & b_{12}M & B_1 & 0 \\ b_{21}M & a_{22}L+b_{22}M+N(\underline{U},\underline{V}) & B_2 & b_{24}M \\ B_1^T & B_2^T & 0 & 0 \\ 0 & 0 & 0 & a_{44}L+N(\underline{U},\underline{V}) \end{bmatrix}\begin{bmatrix}\underline{U}\\ \underline{V}\\ \underline{P}\\ \underline{\theta}\end{bmatrix}=\begin{bmatrix}0\\0\\0\\0\end{bmatrix} \quad (3.25)$$

where

$$a_{11}=\frac{1}{Re}\frac{\rho_f}{\rho_{nf}}\frac{1}{(1-\phi)^{2.5}}=a_{22},$$
$$a_{44}=\frac{\alpha_{nf}}{\alpha_f}\frac{1}{RePr},$$

$$b_{11} = \frac{\rho_f}{\rho_{nf}} \frac{\sigma_{nf}}{\sigma_f} \frac{Ha^2}{Re} \sin^2 \psi,$$

$$b_{12} = -\frac{\rho_f}{\rho_{nf}} \frac{\sigma_{nf}}{\sigma_f} \frac{Ha^2}{Re} \sin \psi \cos \psi = b_{21},$$

$$b_{22} = \frac{\rho_f}{\rho_{nf}} \frac{\sigma_{nf}}{\sigma_f} \frac{Ha^2}{Re} \cos^2 \psi,$$

$$b_{24} = Ri \frac{\rho_f}{\rho_{nf}} \left(1 - \phi + \frac{\rho_s \beta_s}{\rho_f \beta_f} \phi\right).$$

In the block matrix (3.25), L, M and N represent the Laplace, mass and convective matrix respectively, B_1 and B_2 are the pressure matrices and B_1^T, B_2^T are their corresponding transpose. Velocity components and temperature are discretized by Q_2-element of 3rd order accuracy and pressure is approximated by P_1^{disc}-element of 2nd order accuracy (see [27] for details). After putting the approximations in the above equations, residual for each of the governing equations is obtained. The non-linear terms in the governing system of equations are linearized by Picard iteration method.

The convergence of solution is obtained when the relative errors for each variable satisfy the given convergence criteria:

$$\left| \frac{\Gamma^{n+1} - \Gamma^n}{\Gamma^{n+1}} \right| \leq 10^{-6}. \tag{3.26}$$

where 'n' is the number of iteration and Γ is any dependent variable.

3.4 Code Validation

The present code is validated against the benchmarks results of the reattachment lengths for recirculation region in a horizontal channel with a backward facing step at Reynolds number of 100 as shown in the Table 3.3. Prandtl number is fixed at 6.1. Calculations of forced ($Gr = 0$, $Ri = 0$) and mixed convection ($Gr = 1000$, $Ri = 0.1$) past an adiabatic backward facing step with an isothermal surroundings walls are presented in Table 3.3 which shows that our results are in excellent agreement with results of Refs. [28] - [31].

Ri	Present study	Ref. [28]	Ref. [29]	Ref. [30]	Ref. [31]
0.0	4.96875	4.99	4.99	4.97	4.91
0.1	2.96875	3.05	3.05	2.97	3.10

TABLE 3.3: Reattachment lengths for recirculation region at Reynolds number of 100.

3.5 Results and discussion

Numerical result are shown in terms of isotherms and streamlines distribution in Figure 3.2 - Figure 3.5 for different values of governing parameters. The channel is occupied with Cu nanoparticles. Grashof number has fixed value of 5000 for all calculations.

The effect of varying Reynolds number on the streamlines is shown in the Figure 3.2 while other parameters are kept fixed with $Ha = 20$, $\phi = 0.02$, $\psi = 0°$. Strong flow strength is seen near the upper wall which indicates the high velocity for $Re = 20$ as shown in the Figure 3.2(a). When the Reynolds number increases from 20 to 200, the flow at the corner of the step separate and recirculating cell is obtained behind the step. At the beginning for $Re = 20$, the size of recirculation zone decreases as it can be seen in Figure 3.2(a) and then increases with the increase in Reynolds number which can be shown in Figure 3.2(b) and Figure 3.2(c).

The effect of varying Reynolds number on the isotherms distribution is shown in the Figure 3.3 for inclination angle 0° while keeping other parameters fixed, i.e., $Ha = 20$, $\phi = 0.02$ and $\psi = 0°$. Temperature near the bottom hot wall indicates high heat transfer which gradually declines in the flow away from it. A steep temperature contour around the flow reattachment point can be seen along the bottom wall downstream of the step as shown in Figure 3.3(a) - (c).

The effect of varying Hartmann number with $Re = 100$, $\psi = 0°$, $\phi = 0.02$ on streamlines and isotherms distribution is presented in Figures 3.4 and 3.5. The flow separation is seen behind the step in the absence of magnetic field. Flow separation first decreases for $Ha = 0$ as in Figure 3.4(a) then increases with the increasing values of Hartmann number from 0 to 50 as shown in the Figure 3.4(b) and Figure 3.4(c). For the inclined magnetic field, as the value of Ha increases, suppression of the recirculation zone is observed behind the step.

The effect of varying Hartmann number with $\psi = 0°$, $Re = 100$, $\phi = 0.02$ on the isotherms distribution is shown in Figure 3.5. For the horizontally oriented magnetic field, the less contouring of the isotherm along the lower wall near the step can be seen with increasing Hartmann number. The recirculation zone is restricted to a small region and steepest temperature gradient for the vertical and inclined magnetic field is seen in the zone closer to the step as compared to cases with no-magnetic field.

In Figures 3.6 and 3.7, effect of magnetic field inclination ψ on flow and thermal configuration for inclination angle 0°, 45° and 90° in term of streamlines and isotherms is shown. The effect of magnetic field inclination on streamlines is shown in Figure 3.6. Strong flow strength can be seen near the upper wall of channel due to high velocity. For inclination

angle of $\psi = 45°$, the separated flow region behind the step is smallest as it can be seen in the Figure 3.6(b).

The effect of ψ on isotherms is depicted in Figure 3.7. When the inclination angle of magnetic field increases from 0° to 90°, more clustering of the isotherms can be seen at the bottom wall in the vicinity of the step as shown in Figure 3.7(a) - (c). $\psi = 45°$ provides better local heat transfer enhanced characteristics in the near of the step among different orientations of the magnetic field as it is shown in Figure 3.7(b). Average Nusselt number increases with the increase of inclination angle of magnetic field from 0° to 90°.

Average heat transfer versus Reynolds number is depicted in Figure 3.8. It is clearly shown in the Figure 3.8 that average Nusselt number increases with the increasing value of Reynolds number and this effect is more pronounced in case of nanofluid.

The impact of Hartmann number on the average Nusselt number is depicted in Figure 3.9. Heat transfer rate decreases with increase of Hartmann number in case of pure water and nanofluid as shown in the Figure 3.9.

The effect of ψ on average heat transfer is shown in Figure 3.10. The average heat transfer rate increases as the value of inclination angle increases and this impact is more pronounced in case of nanofluid.

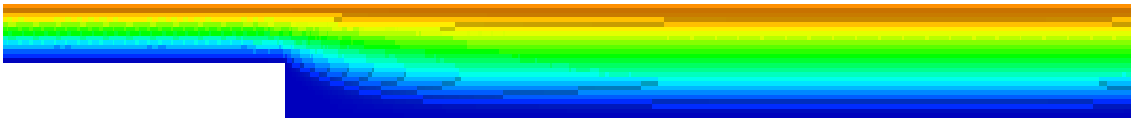

(*a*) $Re = 20$

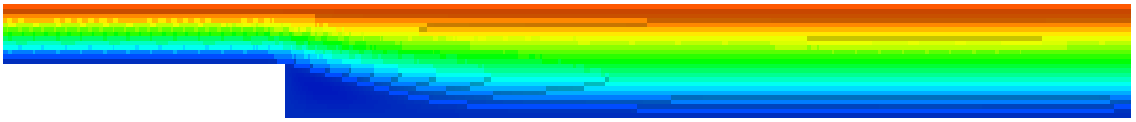

(*b*) $Re = 80$

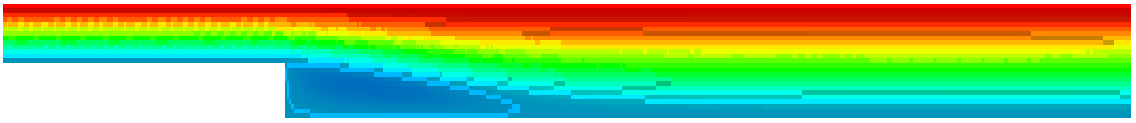

(*c*) $Re = 200$

FIGURE 3.2: Influence of Reynolds number on the streamlines distribution for $\psi = 0°$, $Ha = 20$, $\phi = 0.02$.

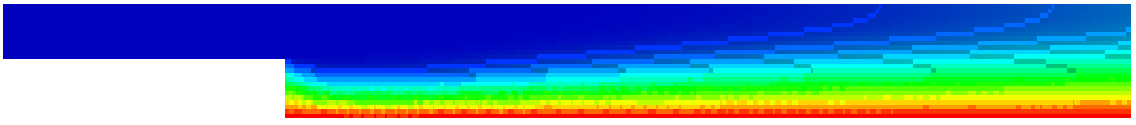

(*a*) $Re = 20$

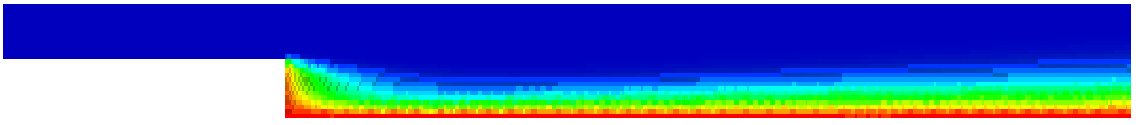

(*b*) $Re = 80$

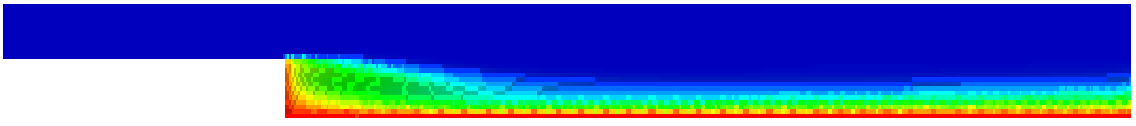

(*c*) $Re = 200$

FIGURE 3.3: Influence of Reynolds number on the isotherms distribution for $\psi = 0°$, $Ha = 20$, $\phi = 0.02$.

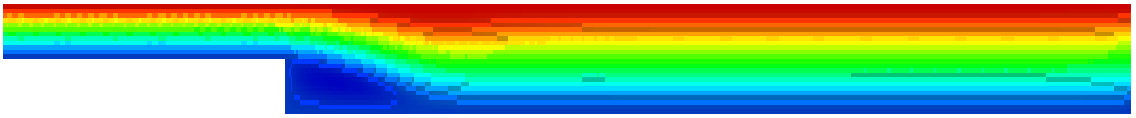

(*a*) $Ha = 0$

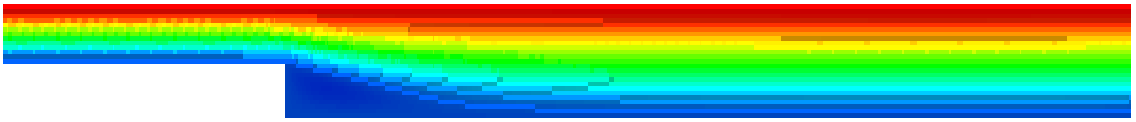

(*b*) $Ha = 20$

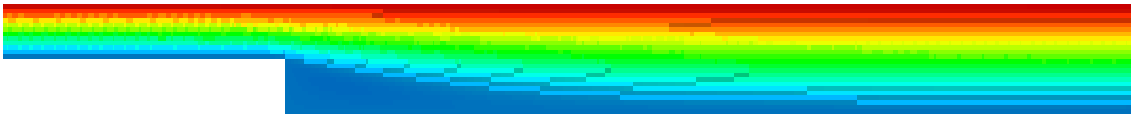

(*c*) $Ha = 50$

FIGURE 3.4: Influence of Hartmann number on the streamlines distribution for $\psi = 0°$, $Re = 100$, $\phi = 0.02$.

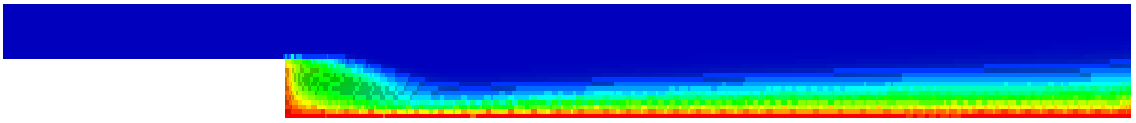

(*a*) $Ha = 0$

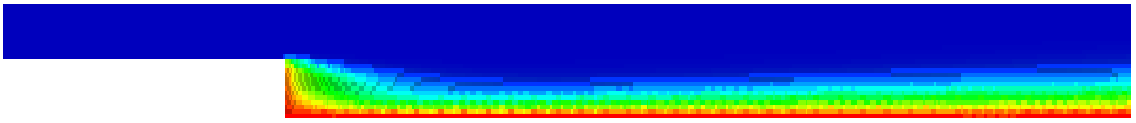

(*b*) $Ha = 20$

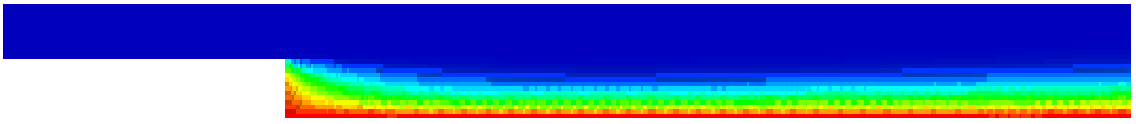

(*c*) $Ha = 50$

FIGURE 3.5: Influence of Hartmann number on the isotherms distribution for $\psi = 0°$, $Re = 100$, $\phi = 0.02$.

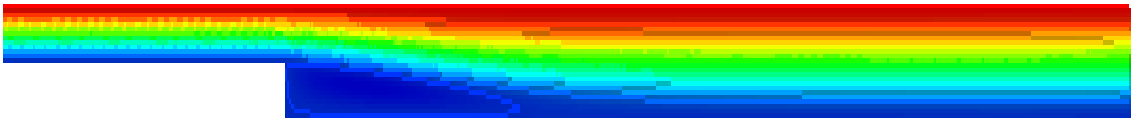

(a) $\psi = 0°$

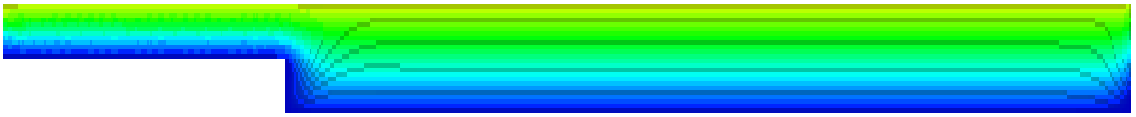

(b) $\psi = 45°$

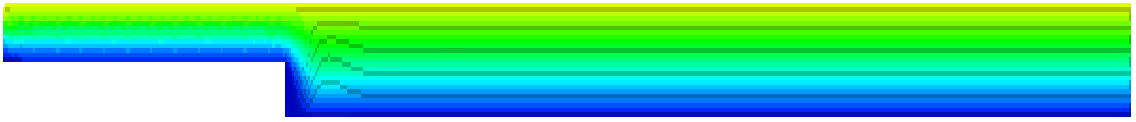

(c) $\psi = 90°$

FIGURE 3.6: Influence of magnetic field inclination on the streamlines distribution for $Ha = 20$, $Re = 200$, $\phi = 0.02$.

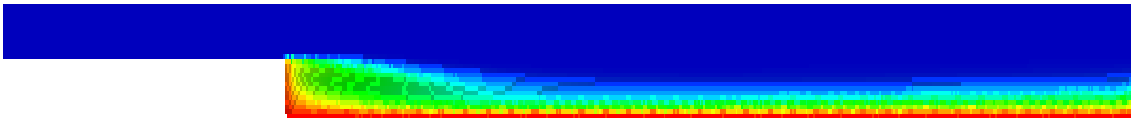

(a) $\psi = 0°$

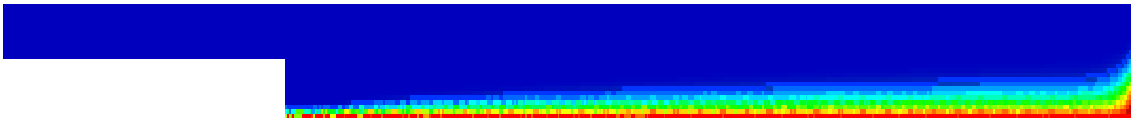

(b) $\psi = 45°$

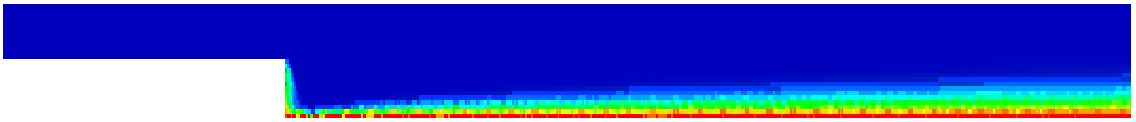

(c) $\psi = 90°$

FIGURE 3.7: Influence of magnetic field inclination on the isotherms distribution for $Ha = 20$, $Re = 200$, $\phi = 0.02$.

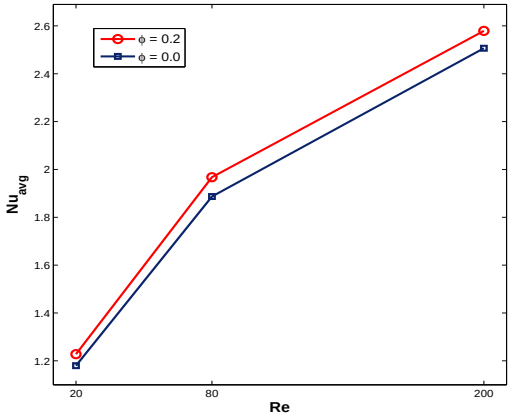

FIGURE 3.8: The effect of Re on average Nusselt number.

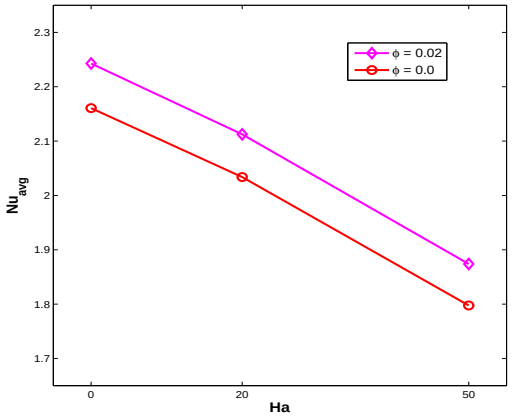

FIGURE 3.9: The effect of Ha on average Nusselt number.

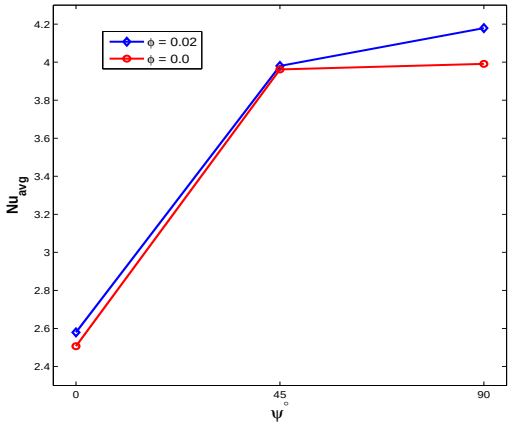

FIGURE 3.10: The effect of inclination angle on average Nusselt number.

Chapter 4

Numerical simulation of mixed convective nanofluid considering internal heat generation/absorption

Based on the literature analysis, in spite of the different studies have been done on backward facing step, there is a definite dearth of information regarding the mixed convective flow over backward facing step with internal heat generation/absorption under the impact of magnetic field inclination. The objective of the present work is to perform a numerical simulation of a two dimensional laminar mixed convective flow over a backward facing step with internal heat generation/absorption using Cu-water as nanofluid.

This chapter investigates the numerical study of laminar mixed convection of nanofluid flow over the backward facing step with the impact of inclined magnetic field and internal heat genaration/absorption. By using appropriate transformation, we derived and solved the system of nonlinear dimensional partial differential equation into coupled dimensionless partial differential equations and solved these equations by the finite element technique together with the Galerkin weighted residual method. The problem convergence is determined. The impact of internal heat generation or absorption in velocity and temperature is discussed and also shown by figures. This work is an extension of the work presented in Chapter 3.

4.1 Mathematical Formulation

Let us consider the laminar two-dimensional flow of an incompressible viscous fluid of an electrically conducting fluid. The channel is filled with Cu nanoparticles with an effect of an inclined magnetic field. Geometry of the physical model is given in Figure 4.1.

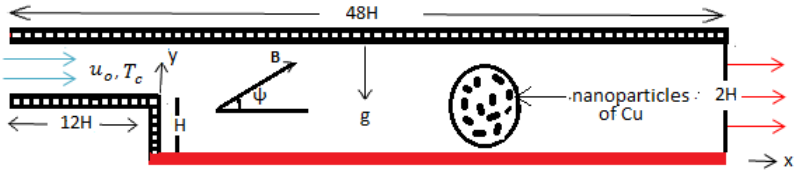

FIGURE 4.1: Geometry of the physical model.

At the inlet, uniform temperature T_c and parabolic velocity are imposed. The bottom walls of the channel downstream of the step is isothermally heated while the other wall are assumed to be adiabatic. The constant thermophysical properties of the fluid [26] are shown in the Table 4.1. Governing equations of momentum, continuity and energy [21] under the above mentioned assumption are given by:

Continuity equation:

$$\frac{\partial u}{\partial x}+\frac{\partial v}{\partial y}=0, \tag{4.1}$$

Momentum equation for u-velocity:

$$u\frac{\partial u}{\partial x}+v\frac{\partial u}{\partial y}=-\frac{1}{\rho_{nf}}\frac{\partial p}{\partial x}+\nu_{nf}\left(\frac{\partial^2 u}{\partial x^2}+\frac{\partial^2 u}{\partial y^2}\right)+\frac{\sigma_{nf}B_0^2}{\rho_{nf}}\left(v\sin(\psi)\cos(\psi)-u\sin^2(\psi)\right), \tag{4.2}$$

Momentum equation for v-velocity:

$$\begin{aligned} u\frac{\partial v}{\partial x}+v\frac{\partial v}{\partial y}=&-\frac{1}{\rho_{nf}}\frac{\partial p}{\partial y}+\nu_{nf}\left(\frac{\partial^2 v}{\partial x^2}+\frac{\partial^2 v}{\partial y^2}\right)+\frac{\sigma_{nf}B_0^2}{\rho_{nf}}\left(u\sin(\psi)\cos(\psi)-v\cos^2(\psi)\right)\\ &+\beta_{nf}g(T-T_c), \end{aligned} \tag{4.3}$$

Energy equation:

$$u\frac{\partial T}{\partial x}+v\frac{\partial T}{\partial y}=\alpha_{nf}\left(\frac{\partial^2 T}{\partial x^2}+\frac{\partial^2 T}{\partial y^2}\right)+\frac{Q_o}{(\rho c_p)_{nf}}(T-T_c). \tag{4.4}$$

Here u, v denotes the velocity component along x-axis and y-axis respectively, the kinematic fluid velocity is ν, the fluid density is ρ, the specific heat is c_p, the fluid thermal conductivity is k, the magnetic field strength is B_0, the electrical conductivity is σ, the expansion coefficient is β, ψ is the inclination angles of magnetic field, Q_o is the heat generation/absorption coefficient, T is the temperature and α is the thermal diffusivity of the nanofluid.
The boundary condition along the channel walls in appropriate forms are

Property	Water	Copper
ρ	997.1	8954
c_p	4179	383
k	0.6	400
β	2.1×10^{-4}	1.67×10^{-5}
σ	0.05	5.97×10^{7}

TABLE 4.1: Thermophysical properties of water and copper [26].

- On the inlet of channel,

$$u = 1, \quad v = 0, \quad T = 0 \tag{4.5}$$

- On the bottom walls,

$$u = 0, \quad v = 0, \quad T = 1. \tag{4.6}$$

- At the outlet,

$$\frac{\partial u}{\partial x} = 0, \quad v = 0, \quad \frac{\partial T}{\partial X} = 0. \tag{4.7}$$

- On the adiabatic wall,

$$u = 0, \quad v = 0, \quad \frac{\partial T}{\partial n} = 0, \tag{4.8}$$

where n represent the normal surface direction.

4.1.1 Non-dimensional Form of the Governing Equations

By using the following dimensionless parameters [21], Eqs. (4.1) - (4.4) are converted into the dimensionless form.

$$q = \frac{Q_o H^2}{(\rho c_p)_{nf} \alpha_{nf}} \quad \text{(Heat generation/absorption parameter)},$$

$$Re = \frac{u_0 H}{\nu_f} \quad \text{(Reynolds number)}.$$

Other dimensionless variables are defined as:

$X = \frac{x}{H}, \quad Y = \frac{y}{H}, \quad U = \frac{u}{u_0}, \quad V = \frac{v}{u_0}, \quad P = \frac{p}{\rho_f u_0^2}, \quad \theta = \frac{T - T_c}{T_h - T_c}, \quad Pr = \frac{\nu_f}{\alpha_f},$

$Gr = \frac{g\beta_f (T_h - T_c) H^3}{\nu_f^2}, \quad Re = \frac{u_0 H}{\nu_f}, \quad Ri = \frac{Gr}{Re^2}, \quad Ha = B_0 H \sqrt{\frac{\sigma_f}{\mu_f}}.$

$$\frac{\partial U}{\partial X}+\frac{\partial V}{\partial Y}=0, \tag{4.9}$$

$$U\frac{\partial U}{\partial X}+V\frac{\partial U}{\partial Y}=-\frac{\partial P}{\partial X}+\frac{1}{Re}\frac{\rho_f}{\rho_{nf}}\frac{1}{(1-\phi)^{2.5}}\left(\frac{\partial^2 U}{\partial X^2}+\frac{\partial^2 U}{\partial Y^2}\right) + \frac{\rho_f}{\rho_{nf}}\frac{\sigma_{nf}}{\sigma_f}\frac{Ha^2}{Re}\left(V\sin(\psi)\cos(\psi)-U\sin^2(\psi)\right), \tag{4.10}$$

$$U\frac{\partial V}{\partial X}+V\frac{\partial V}{\partial Y}=-\frac{\partial P}{\partial Y}+\frac{1}{Re}\frac{\rho_f}{\rho_{nf}}\frac{1}{(1-\phi)^{2.5}}\left(\frac{\partial^2 V}{\partial X^2}+\frac{\partial^2 V}{\partial Y^2}\right)+Ri\frac{\rho_f}{\rho_{nf}}\left(1-\phi+\frac{\rho_s\beta_s}{\rho_f\beta_f}\phi\right)\theta + \frac{\rho_f}{\rho_{nf}}\frac{\sigma_{nf}}{\sigma_f}\frac{Ha^2}{Re}\left(U\sin(\psi)\cos(\psi)-V\cos^2(\psi)\right), \tag{4.11}$$

$$U\frac{\partial \theta}{\partial X}+V\frac{\partial \theta}{\partial Y}=\frac{\alpha_{nf}}{\alpha_f}\frac{1}{RePr}\left(\frac{\partial^2 \theta}{\partial X^2}+\frac{\partial^2 \theta}{\partial Y^2}\right)+\frac{q}{RePr}\theta \tag{4.12}$$

Here U, V denotes the dimensionless velocity component along X and Y dimensionless coordinates respectively, q is the heat source parameter and θ represent the non-dimensional temperature.

The dimensionless boundary condition along the channel walls in appropriate forms are as follows

- On the inlet side of the channel:

$$U=1, \quad V=0, \quad \theta=0. \tag{4.13}$$

- On the bottom wall:

$$U=0, \quad V=0, \quad \theta=1. \tag{4.14}$$

- On the outlet side of the channel:

$$\frac{\partial U}{\partial X}=0, \quad V=0, \quad \frac{\partial \theta}{\partial X}=0. \tag{4.15}$$

- On the rest of walls of channel:

$$U=0, \quad V=0, \quad \frac{\partial \theta}{\partial n}=0, \tag{4.16}$$

  where n represent the surface normal direction.

4.2 Numerical Solution

The basic idea of finite element method is to transform the following equations into the variational or weak form. The whole domain is discretized into quadrilateral elements. The systems of coupled nonlinear partial differentials Eqs. (4.9) - (4.12) together with the boundary conditions (4.13) - (4.16) has been solved numerically by Galerkin weighted residual method of finite element formulation. First, we established the weak formulation of the governing equations and then approximated the solution utilizing the Galerkin approximation procedure.

4.2.1 Variational form and Governing Matrix

The distinguishing feature of finite element method is that the equations are multiplied by a test function before they are integrated over the whole domain Ω.
Let W = ($H^1(\Omega)$, $H^1(\Omega)$, $H^1(\Omega)$) be the test space for velocity components and temperature and Q = $L^2(\Omega)$ is the test space for pressure.
A variational form is as follows
Strong form:

$$\frac{\partial U}{\partial X} + \frac{\partial V}{\partial Y} = 0, \tag{4.17}$$

$$U\frac{\partial U}{\partial X} + V\frac{\partial U}{\partial Y} = -\frac{\partial P}{\partial X} + \frac{1}{Re}\frac{\rho_f}{\rho_{nf}}\frac{1}{(1-\phi)^{2.5}}\left(\frac{\partial^2 U}{\partial X^2} + \frac{\partial^2 U}{\partial Y^2}\right) + \frac{\rho_f}{\rho_{nf}}\frac{\sigma_{nf}}{\sigma_f}\frac{Ha^2}{Re}\left(V\sin(\psi)\cos(\psi) - U\sin^2(\psi)\right), \tag{4.18}$$

$$U\frac{\partial V}{\partial X} + V\frac{\partial V}{\partial Y} = -\frac{\partial P}{\partial Y} + \frac{1}{Re}\frac{\rho_f}{\rho_{nf}}\frac{1}{(1-\phi)^{2.5}}\left(\frac{\partial^2 V}{\partial X^2} + \frac{\partial^2 V}{\partial Y^2}\right) + Ri\frac{\rho_f}{\rho_{nf}}\left(1 - \phi + \frac{\rho_s\beta_s}{\rho_f\beta_f}\phi\right)\theta + \frac{\rho_f}{\rho_{nf}}\frac{\sigma_{nf}}{\sigma_f}\frac{Ha^2}{Re}\left(U\sin(\psi)\cos(\psi) - V\cos^2(\psi)\right), \tag{4.19}$$

$$U\frac{\partial \theta}{\partial X} + V\frac{\partial \theta}{\partial Y} = \frac{\alpha_{nf}}{\alpha_f}\frac{1}{RePr}\left(\frac{\partial^2 \theta}{\partial X^2} + \frac{\partial^2 \theta}{\partial Y^2}\right) + \frac{q}{RePr}\theta \tag{4.20}$$

A variational form is given as

Find (U, V, P, θ) ϵ W $\times$ Q such that

$$\int_\Omega \left(U\frac{\partial U}{\partial X}+V\frac{\partial U}{\partial Y}\right)\ w\ d\Omega-\frac{1}{Re}\frac{\rho_f}{\rho_{nf}}\frac{1}{(1-\phi)^{2.5}}\int_\Omega\left(\frac{\partial^2 U}{\partial X^2}+\frac{\partial^2 U}{\partial Y^2}\right)\ w\ d\Omega$$
$$-\frac{\rho_f}{\rho_{nf}}\frac{\sigma_{nf}}{\sigma_f}\frac{Ha^2}{Re}\int_\Omega\left(V\sin(\psi)\cos(\psi)-U\sin^2(\psi)\right)\ w\ d\Omega+\int_\Omega\frac{\partial P}{\partial X}\ w\ d\Omega=0, \quad (4.21)$$

$$\int_\Omega \left(U\frac{\partial V}{\partial X}+V\frac{\partial V}{\partial Y}\right)\ w\ d\Omega-\frac{1}{Re}\frac{\rho_f}{\rho_{nf}}\frac{1}{(1-\phi)^{2.5}}\int_\Omega\left(\frac{\partial^2 V}{\partial X^2}+\frac{\partial^2 V}{\partial Y^2}\right)\ w\ d\Omega$$
$$-\frac{\rho_f}{\rho_{nf}}\frac{\sigma_{nf}}{\sigma_f}\frac{Ha^2}{Re}\int_\Omega\left(U\sin(\psi)\cos(\psi)-V\cos^2(\psi)\right)\ w\ d\Omega$$
$$-Ri\frac{\rho_f}{\rho_{nf}}\left(1-\phi+\frac{\rho_s\beta_s}{\rho_f\beta_f}\phi\right)\int_\Omega\theta\ w\ d\Omega+\int_\Omega\frac{\partial P}{\partial Y}\ w\ d\Omega=0, \quad (4.22)$$

$$\int_\Omega\left(\frac{\partial U}{\partial X}+\frac{\partial V}{\partial Y}\right)\ q\ d\Omega=0, \quad (4.23)$$

$$\int_\Omega\left(U\frac{\partial\theta}{\partial X}+V\frac{\partial\theta}{\partial Y}\right)\ w\ d\Omega-\frac{\alpha_{nf}}{\alpha_f}\frac{1}{RePr}\int_\Omega\left(\frac{\partial^2\theta}{\partial X^2}+\frac{\partial^2\theta}{\partial Y^2}\right)\ w\ d\Omega-\frac{q}{RePr}\int_\Omega\theta\ w\ d\Omega. \quad (4.24)$$

for all $(w,\ q)\ \epsilon$ W $\times$ Q.

Let $U\approx U_h$, $V\approx V_h$, $\theta\approx\theta_h$, $P\approx P_h$.

$w\approx w_h$, $q\approx q_h$.

The Galerkin weighted residual method transform the nonlinear equation given below

$$\frac{1}{Re}\frac{\rho_f}{\rho_{nf}}\frac{1}{(1-\phi)^{2.5}}\int_\Omega\left(\frac{\partial U_h}{\partial X}\frac{\partial w_h}{\partial X}+\frac{\partial U_h}{\partial Y}\frac{\partial w_h}{\partial Y}\right)\ d\Omega+\int_\Omega\left(U_h\frac{\partial U_h}{\partial X}+V_h\frac{\partial U_h}{\partial Y}\right)\ w_h\ d\Omega$$
$$-\frac{\rho_f}{\rho_{nf}}\frac{\sigma_{nf}}{\sigma_f}\frac{Ha^2}{Re}\int_\Omega\left(V_h\sin(\psi)\cos(\psi)-U_h\sin^2(\psi)\right)\ w_h\ d\Omega+\int_\Omega\frac{\partial P_h}{\partial X}\ w_h\ d\Omega=0, \quad (4.25)$$

$$\frac{1}{Re}\frac{\rho_f}{\rho_{nf}}\frac{1}{(1-\phi)^{2.5}}\int_\Omega\left(\frac{\partial V_h}{\partial X}\frac{\partial w_h}{\partial X}+\frac{\partial V_h}{\partial Y}\frac{\partial w_h}{\partial Y}\right)\ d\Omega+\int_\Omega\left(U_h\frac{\partial V_h}{\partial X}+V_h\frac{\partial V_h}{\partial Y}\right)\ w_h\ d\Omega$$
$$-Ri\frac{\rho_f}{\rho_{nf}}\left(1-\phi+\frac{\rho_s\beta_s}{\rho_f\beta_f}\phi\right)\int_\Omega\theta_h\ w_h\ d\Omega$$
$$-\frac{\rho_f}{\rho_{nf}}\frac{\sigma_{nf}}{\sigma_f}\frac{Ha^2}{Re}\int_\Omega\left(U_h\sin(\psi)\cos(\psi)-V_h\cos^2(\psi)\right)\ w_h\ d\Omega+\int_\Omega\frac{\partial P_h}{\partial Y}\ w_h\ d\Omega=0, \quad (4.26)$$

$$\int_\Omega\left(\frac{\partial U_h}{\partial X}+\frac{\partial V_h}{\partial Y}\right)\ q_h\ d\Omega=0, \quad (4.27)$$

$$\frac{\alpha_{nf}}{\alpha_f}\frac{1}{RePr}\int_\Omega\left(\frac{\partial\theta_h}{\partial X}\frac{\partial w_h}{\partial X}+\frac{\partial\theta_h}{\partial Y}\frac{\partial w_h}{\partial Y}\right)\ d\Omega+\int_\Omega\left(U_h\frac{\partial\theta_h}{\partial X}+V_h\frac{\partial\theta_h}{\partial Y}\right)\ w_h\ d\Omega-\frac{q}{RePr}\theta_h w_h\ d\Omega=0. \quad (4.28)$$

Using the FEM approximations of U_h, V_h, P_h and θ_h, the fully discrete block system reads the following:

$$\begin{bmatrix} A_{11} & b_{12}M & B_1 & 0 \\ b_{21}M & A_{22} & B_2 & b_{24}M \\ B_1^T & B_2^T & 0 & 0 \\ 0 & 0 & 0 & A_{44} \end{bmatrix} \begin{bmatrix} \underline{U} \\ \underline{V} \\ \underline{P} \\ \underline{\theta} \end{bmatrix} = \begin{bmatrix} 0 \\ 0 \\ 0 \\ 0 \end{bmatrix}, \tag{4.29}$$

where

$$\begin{aligned} A_{11} &= a_{11}L + b_{11}M + N(\underline{U}, \underline{V}), \\ A_{22} &= a_{22}L + b_{22}M + N(\underline{U}, \underline{V}), \\ A_{44} &= b_{44}M + N(\underline{U}, \underline{V}), \\ a_{11} &= \frac{1}{Re}\frac{\rho_f}{\rho_{nf}}\frac{1}{(1-\phi)^{2.5}} = a_{22}, \\ a_{44} &= \frac{\alpha_{nf}}{\alpha_f}\frac{1}{RePr}, \\ b_{11} &= \frac{\rho_f}{\rho_{nf}}\frac{\sigma_{nf}}{\sigma_f}\frac{Ha^2}{Re}\sin^2\psi, \\ b_{12} &= -\frac{\rho_f}{\rho_{nf}}\frac{\sigma_{nf}}{\sigma_f}\frac{Ha^2}{Re}\sin\psi\cos\psi = b_{21}, \\ b_{22} &= \frac{\rho_f}{\rho_{nf}}\frac{\sigma_{nf}}{\sigma_f}\frac{Ha^2}{Re}\cos^2\psi, \\ b_{24} &= Ri\frac{\rho_f}{\rho_{nf}}\left(1-\phi+\frac{\rho_s\beta_s}{\rho_f\beta_f}\phi\right), \\ b_{44} &= -\frac{1}{RePr}q. \end{aligned}$$

L, M, N in the block matrix (4.29) represents the Laplace, mass and convective matrices respectively, B_1 and B_2 are the pressure matrices and B_1^T, B_2^T are their corresponding transpose.

Velocity components and temperature are discretized by Q_2-element and pressure is approximated by P_1^{disc}-element (see [27] for details). The non-linear terms in the governing system of equations are linearized by Picard iteration method.

The convergence of our solution is assumed when the relative error for each of the variables satisfy the given convergence criteria:

$$\left|\frac{\Gamma^{n+1}-\Gamma^{n}}{\Gamma^{n+1}}\right| \leq 10^{-6}. \tag{4.30}$$

Where 'n' is the number of iteration and Γ is any dependent variable.

4.3 Results and discussion

Application of FEM is performed to study the effect of thermal boundary conditions on combined convection heat transfer and fluid flow. In this section, numerical result are presented in terms of streamline and isotherm distribution for different value of physical parameters. The channel is filed with Cu-water nanofluid. The governing parameters are Hartmann number ($0 \leq Ha \leq 20$), Reynolds number ($20 \leq Re \leq 200$), solid volume fraction ($0 \leq \phi \leq 0.04$) and magnetic field inclination angle($0^{\circ} \leq \psi \leq 90^{\circ}$). The considered values of heat generation/absorption parameter are taken as (-10, -5, 0, 5, 10). Prandtl number is fixed at 6.1 and Grashof number is also fixed at 5000. Numerical simulation of streamlines and isotherms for above mentioned parameters are displayed and the value of average Nusselt number has been calculated.

Figure 4.2 and Figure 4.3 shows the temperature and velocity field for various values of Re. In Figure 4.2, the effect of varying Re on streamlines is shown. Flow strength due to high velocity can be seen on the above wall of channel in Figure 4.2(a) for $Re = 20$. When the Reynolds number increases Figure 4.2(a) - (c), the flow at the corner of the step separates and a recirculation zone is observed behinds the step. For $Re = 20$, the size of recirculation zone decreases and then increases for $Re = 80$ and $Re = 200$ and with the increases in the Reynolds number, the maximum value of the stream function increases.

The impact of Reynolds number on the isotherms is depicted in the Figure 4.3. Temperature near the heated wall shows the thickness of thermal boundary layer. Average Nusselt number increases with increasing of Reynolds number. When Reynolds number increases as in Figure 4.3(a) - (c), more contouring of the isotherm can be shown in the lower wall in the vicinity of the step. Among different orientations of magnetic field, $\psi = 45^{\circ}$ provides better heat transfer enhanced characteristics in the vicinity of the step compared to horizontal and vertical alignment as shown in Figure 4.3(b).

The effect of internal heat generation/absorption parameter is shown in Figure 4.4 and Figure 4.5. Here, we considered three cases, i.e., heat generation ($q > 0$), heat absorption (q

< 0) and $q = 0$ i.e. no heat generation or absorption. Heat generation/absorption parameter does not effect the streamlines distribution. The effect of heat generation/absorption parameter on isotherms distribution is shown in Figure 4.5. There is shown a slight increase in heat transfer in case of heat absorption whereas a decrease has been observed in case of heat generation. Average Nusselt number decreases with an increase in heat generation parameter. Quantitative changes can be seen through graph.

The influence of magnetic field inclination through streamlines and isotherms distribution is shown in Figure 4.6 and Figure 4.7. For inclination angle of $\psi = 45°$, the separated flow region behind the step is smallest as it can be seen in the Figure 4.6(b). Heat transfer rate seems to be increased with an increase in inclination angle of magnetic field from 0° to 90°.

Average Nusselt number verses Reynolds number is shown in Figure 4.8. Average heat transfer increases as the value of Reynolds number seems to be increased at $\psi = 45°$.
The effect of internal heat generation on average Nusselt number is shown in Figure 4.9. As we increase the value of q from -10 to 10, average heat transfer decreases as shown in Figure 4.9.

Average Nusselt number verses magnetic field inclination is depicted in the Figure 4.10. The graph clearly shows that with an increase in an inclination of magnetic field, i.e., from 0° to 90°, heat transfer rate increases.

The impact of ϕ on averaged Nusselt number with various magnetic field inclination ($0° \leq \psi \leq 90°$) as a function of nanoparticle volumes fraction is shown graphically in Figure 4.11. It is clear from the graph that when solid volume fraction increase, average Nusselt number is also increases and this effect is more pronounced with higher values of magnetic field inclination.

Figure 4.12 and Figure 4.13 illustrates the strong effect of solid volume fraction ϕ in various cases, i.e., 0 (pure water), 0.02 and 0.04. In Figure 4.12, the effect of solid volume fraction is discussed for $Ri = 0.125$ while other parameters has fixed values, i.e., $Ha = 20$, $\psi = 45°$, $Pr = 6.1$ and $Re = 200$. Average Nusselt number for the dominating forced convection shows that curve falls down with an increase in heat generation parameter.
Figure 4.13 considers $Ri = 1$ (mixed convection) where Nusselt number decreases by increasing the heat generation parameter.

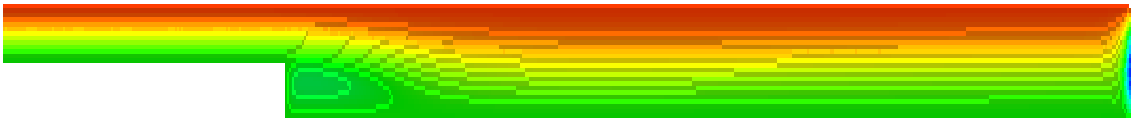

(*a*) $Re = 20$

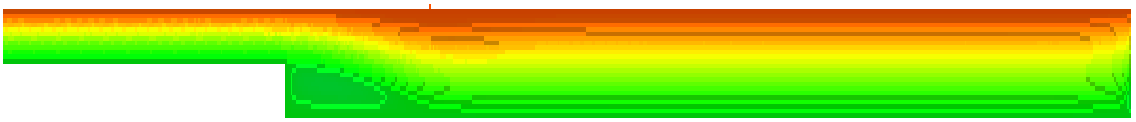

(*b*) $Re = 80$

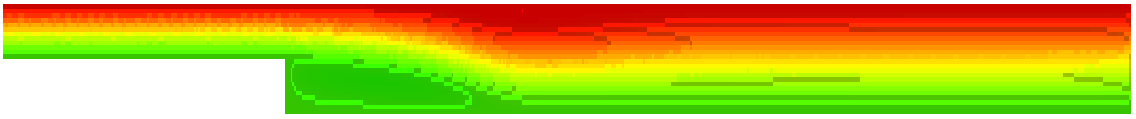

(*c*) $Re = 200$

FIGURE 4.2: Influence of Reynolds number on the streamlines distribution for $\psi = 45°$, $Ha = 0$, $\phi = 0.02$, $q = 5$.

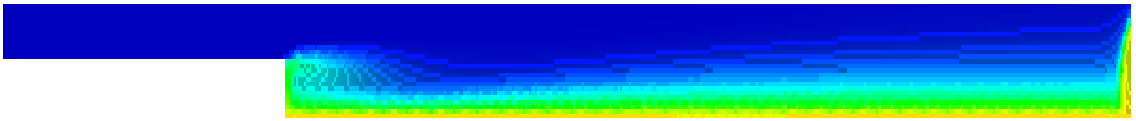

(*a*) $Re = 20$

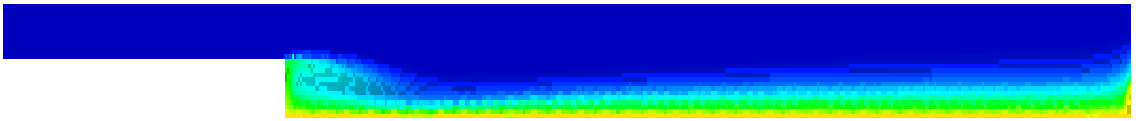

(*b*) $Re = 80$

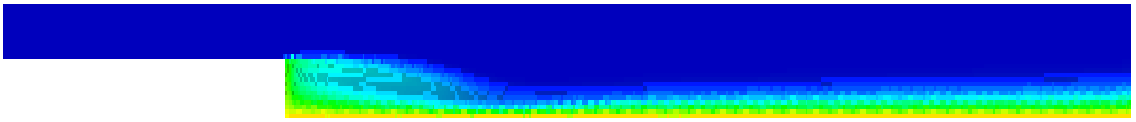

(*c*) $Re = 200$

FIGURE 4.3: Influence of Reynolds number on the isotherms distribution for $\psi = 45°$, $Ha = 0$, $\phi = 0.02$, $q = 5$.

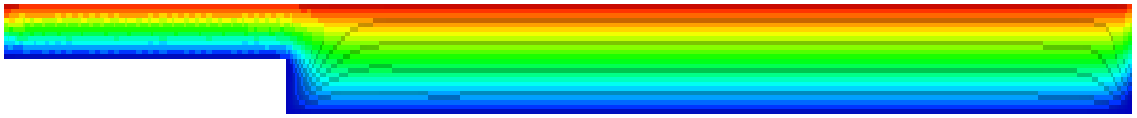

(*a*) $q = -10$

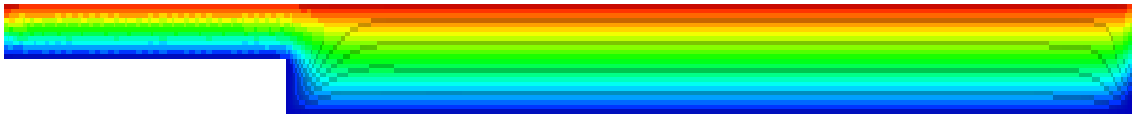

(*b*) $q = -5$

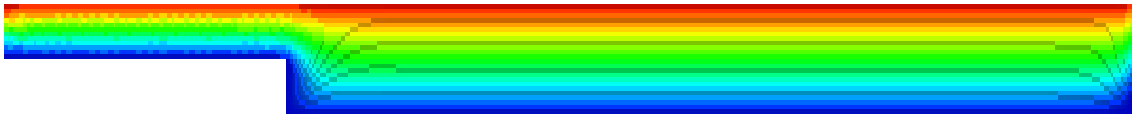

(*c*) $q = 0$

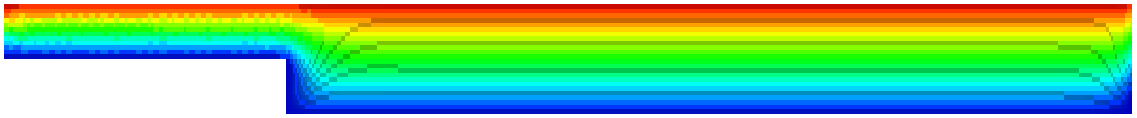

(*d*) $q = 5$

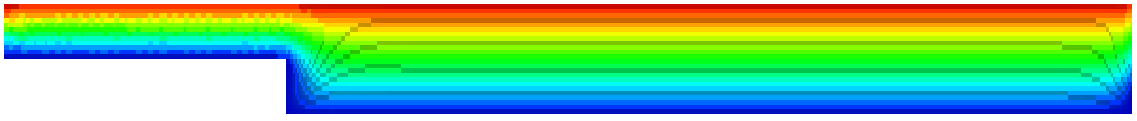

(*e*) $q = 10$

FIGURE 4.4: Influence of q on the streamlines distribution for $Re = 200$, $Ha = 20$, $\psi = 45°$.

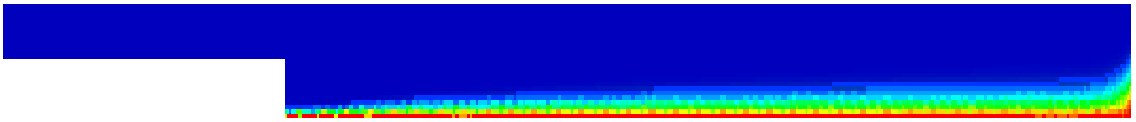

(*a*) $q = -10$

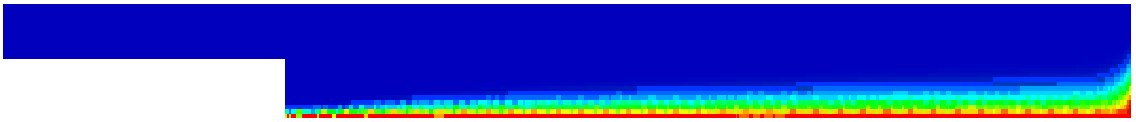

(*b*) $q = -5$

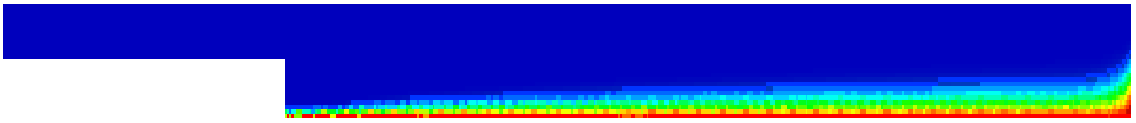

(*c*) $q = 0$

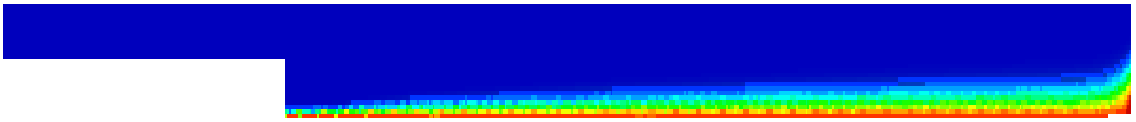

(*d*) $q = 5$

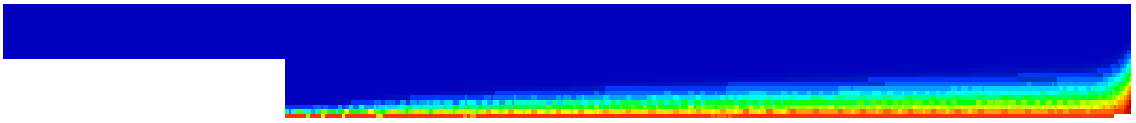

(*e*) $q = 10$

FIGURE 4.5: Influence of q on the isotherms distribution for $Re = 200$, $Ha = 20$, $\psi = 45°$.

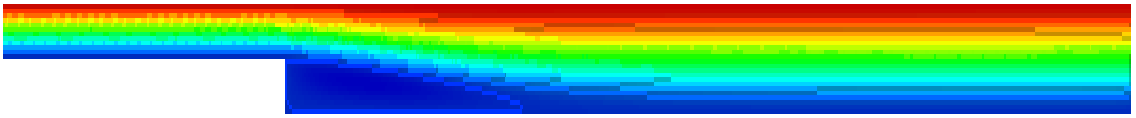

(*a*) $\psi = 0°$

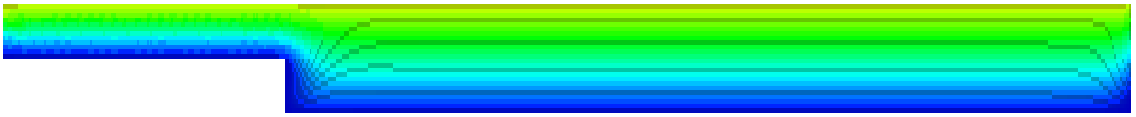

(*b*) $\psi = 45°$

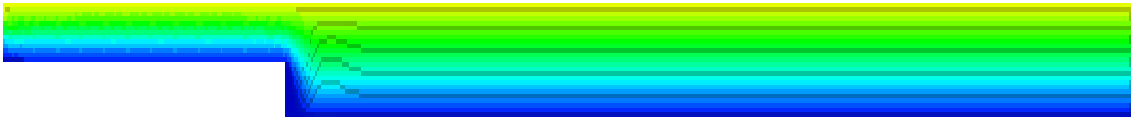

(*c*) $\psi = 90°$

FIGURE 4.6: Influence of inclination angle on the streamlines distribution for $Re = 200$, $Ha = 20$, $q = 10$.

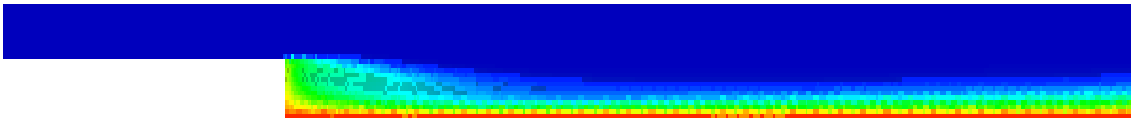

(*a*) $\psi = 0°$

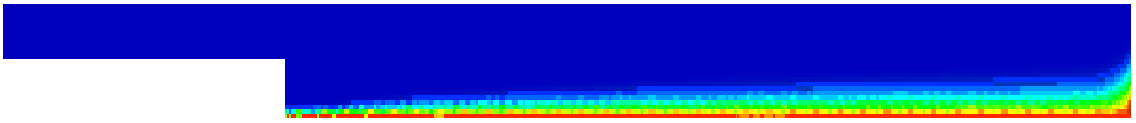

(*b*) $\psi = 45°$

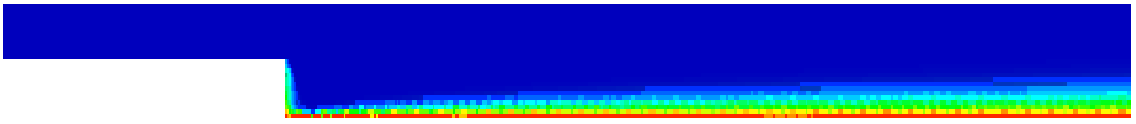

(*c*) $\psi = 90°$

FIGURE 4.7: Influence of inclination angle on the isotherms distribution for $Re = 200$, $Ha = 20$, $q = 10$.

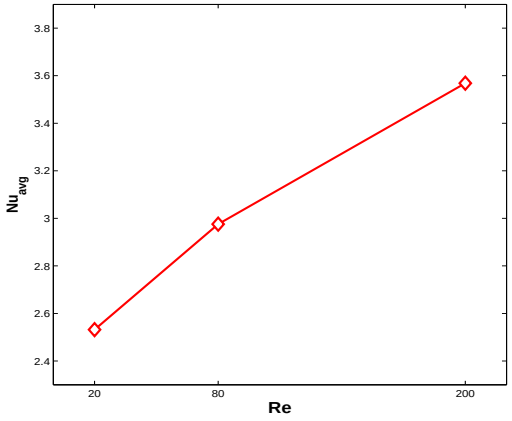

FIGURE 4.8: The effect of Re on average Nusselt number.

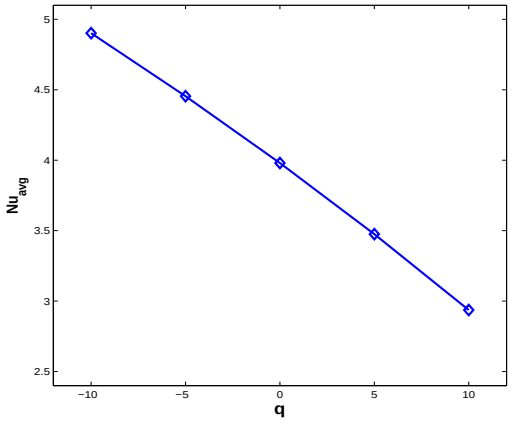

FIGURE 4.9: The effect of q on average Nusselt number.

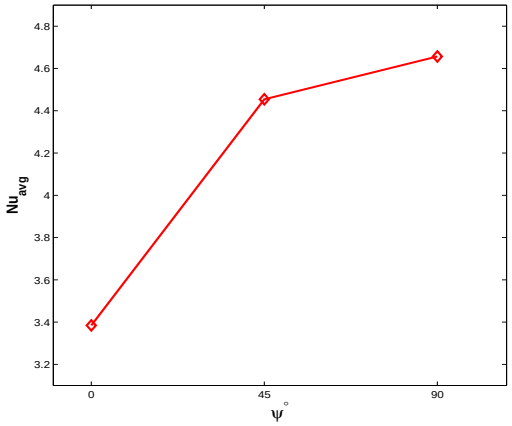

FIGURE 4.10: The effect of ψ on average Nusselt number.

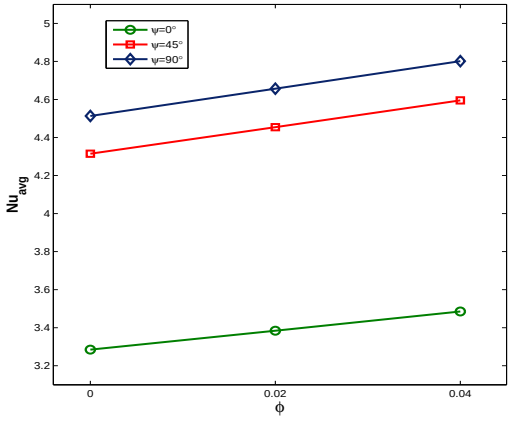

FIGURE 4.11: The effect of ϕ on average Nusselt number.

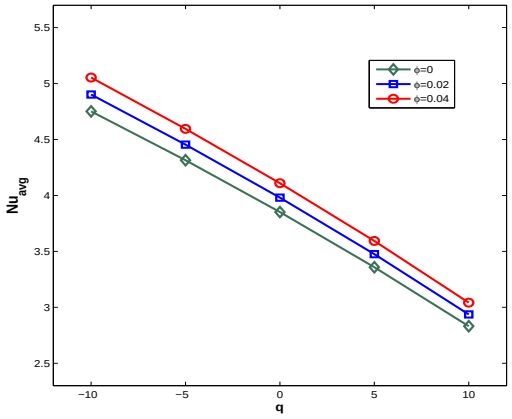

FIGURE 4.12: The influence of ϕ on average Nusselt number for $Ri = 0.125$.

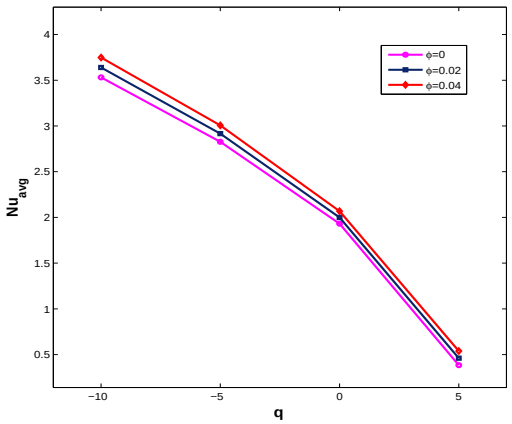

FIGURE 4.13: The influence of ϕ on average Nusselt number for $Ri = 1$.

Chapter 5

Conclusion

In this dissertation, the analysis of laminar mixed convection of Cu-water nanofluid over the backward facing step under the influence of an inclination angle of magnetic field and internal heat generation/aborption is investigated. The governing dimensional PDEs are converted into dimensionless PDEs by using dimensionless parameters and these equations are discretized by Galarkin finite elements method. Different values for the heat generation parameter, Reynolds number, magnetic field inclination and ϕ have been analyzed for the temperature field and also for heat transfer rate while Pr is fixed at 6.1. Non-dimensional quantities like velocity, temperature, Reynolds number and Nusselt number are shown graphically and their numerical values are investigated.

We extended the work of Selimefendigil *et al.* [26], with an idea of internal heat generation/absorption parameters to incorporate as shown in energy equation. We discussed the heat generation/absorption parameters considering some fixed values of it and the effect of different parameter on it. The Numerical results for the dimensionless velocity and dimensionless temperature are studied and depicted graphically for the effect of appropriate parameters.
The conclusions of the numerical simulations lead to the following points.

- Average Nusselt number increases as the Reynolds number increases for magnetic field inclination range $0^\circ \leq \psi \leq 90^\circ$ while keeping all the other parameters constant.
- Heat transfer rate decreases with the increase in Hartmann number for magnetic field inclination in specific range $0^\circ \leq \psi \leq 90^\circ$ while keeping all the other parameters constant.

- Average Nusselt number decreases with an increase in heat generation and increases with an increase in absorption parameter and this effect is more pronounced in case of nanofluid while keeping all the other parameters fixed.
- Heat transfer increases with an increase in the solid volume fraction and this effect is more pronounced with higher values of inclinations angles of magnetic field while other parameters kept constant.
- Average Nusselt number increases with the increase in magnetic field inclination while keeping all the other parameters fixed.

5.1 Future scope

In future, this problem may be extended in many direction focusing on the following ideas.

- The impact of porous media.
- Perform non-stationary simulations of nanofluid in backward facing step.
- Apply the higher order finite elements in space.
- Apply the Galerkin discretization scheme for temporal discretization.

Bibliography

[1] D. Ratha and A. Sarkar. Analysis of flow over backward facing step with transition. *International Journal of Thermal Sciences*, 10:1–10, 2014.

[2] H. A. Mulaweh. A review of research on laminar mixed convection flow over backward- and forward-facing steps. *International Journal of Thermal Sciences*, 42:897–909, 2003.

[3] D. Barkley, M. Gomes, and R. Henderson. Three-dimensional instability in flow over a backward-facing step. *Fluid Mechanics*, 473:167–190, 2002.

[4] B. Armaly, F. Durst, J. Pereier, and B. Schonung. Experimental and theoretical investigation of backward-facing step flow. *Fluid Mechanics*, 127:473–496, 1983.

[5] E. A. Nada. Applications of nanofluids for heat transfer enhancement of separated flows encountered in backward facing step. *Heat and Fluid Flow*, 29:242–249, 2008.

[6] B. Ghasemi, S. Aminossadati, and A. Raisi. Magnetic field effect on natural convection in nanofluid-filled square enclosure. *International Journal of Thermal Sciences.*, 50: 1748–1756, 2011.

[7] F. Selimefendigil and H. Oztop. Numerical study of MHD mixed convection in a nanofluid filled lid driven square enclosure with a rotating cylinder. *International Journal Heat Mass Transfer*, 78:741–754, 2014.

[8] A. Kherbeet, H. Mohammed, K. Munisamy, and B. Salman. The effect of step height of microscale backward-facing step on mixed convection nanofluid flow and heat transfer characteristics. *International Journal of Heat and Mass Transfer*, 68:554–566, 2014.

[9] A. Aswadi, H. Mohammed, and N. Shuaib. Laminar forced convection flow over a backward facing step using nanofluids. *International Communication in Heat and Mass Transfer*, 37:950–957, 2010.

[10] F. Selimefendigil and H. Oztop. Numerical study of MHD mixed convection in a nanofluid filled lid driven square enclosure with a rotating cylinder. *International Journal of Heat and Mass Transfer*, 78:741–754, 2014.

[11] M. Pirmohammadi and M. Ghassemi. Effect of magnetic field on convection heat transfer inside a tilted square enclosure. *International Communication in Heat and Mass Transfer*, 36:776–780, 2009.

[12] H. Abbasi and S. Nassrallah. MHD flow and heat transfer in a backward-facing step. *International Communication in Heat and Mass Transfer*, 34:231–237, 2007.

[13] Z. Mehrez, A. Cafsi, A. Belghith, and P. Quere. MHD effects on heat transfer and entropy generation of nanofluid flow in an open cavity. *Magnetism and Magnetic Materials*, 364:214–224, 2015.

[14] G. Zheng, M. Ha, H. Yoon, and Y. Park. A numerical study on mixed convection in a lid-driven cavity with a circular cylinder. *Mechanical Science and Technology*, 27: 273–286, 2013.

[15] L. Saha, M. Somadder, and K. Salah Uddin. Mixed convection heat transfer in a lid driven cavity with wavy bottom surface. *American Journal of Applied Mathematics*, 5: 92–101, 2013.

[16] R. Nasrin, M. A. Alim, and A. J. Chamkha. Modeling of mixed convective heat transfer utilizing nanofluid in a double lid-driven chamber with internal heat generation. *International Journal of Numerical Methods for Heat and Fluid Flow*, 24:36–57, 2014.

[17] G. M. Pavithra and B. J. Gireesha. Effect of internal heat generation/absorption on dusty fluid flow over an exponentially stretching sheet with viscous dissipation. *Journal of Mathematics*, 2013:1–10, 2013.

[18] M. A. Hamad and I. Pop. Scaling transformations for boundary layer flow near the stagnation-point on a heated permeable stretching surface in a porous medium saturated with a nanofluid and heat generation/absorption effects. *Transport in Porous Media*, 87:25–39, 2010.

[19] M. K. Das and R. K. Tiwari. Heat transfer augmentation in a two-sided lid-driven differentially heated square cavity utilizing nanofluids. *International Journal of Heat and Mass Transfer*, 50:2002–2018, 2007.

[20] S. M. Aminossadati and M. Ghasemi. Natural convection cooling of a localised heat source at the bottom of nanofluid-filled enclosure. *European Journal of Mechanics-B/Fluids*, 28:630–640, 2009.

[21] E. B. Ogut. Natural convection of water-based nanofluids in an inclined encclosure with a heat source. *International Journal of Thermal Sciences*, 48:2063–2073, 2009.

[22] M. A. Samad and M. Mohebujjaman. MHD heat and mass transfer free convection flow along a vertical stretching sheet in presence of magnetic field with heat generation. *Research Journal of Applied Sciences*, 1:98–106, 2009.

[23] E. Elbashbeshy and D. Aldawody. Heat transfer over an unsteady stretching surface with variable heat flux in the presence of a heat source or sink. *Computers and Mathematics with Applications*, 60:2806–2811, 2010.

[24] J. H. Ferziger and M. Peric. Computational methods for fluid dynamics. *Springer*, 3, 2002.

[25] R. Lohner. Applied computational fluid dynamics techniques. *Wiley*, 2, 2008.

[26] F. Selimefendigil and H. Oztop. Influence of inclination angle of magnetic field on mixed convection of nanofluid flow over a backward facing step. *Advanced Powder Technology*, 25:1663–1675, 2015.

[27] S. Hussain, F. Schieweck, and S. Turek. Efficient Newton multigrid solution techniques for higher order space time Galerkin discretizations of incompressible flow. *Applied Numerical Mathematics*, 83:51–71, 2014.

[28] K. Khanafer, B. Al-Azmi, A. Al-Shammari, and I. Pop. Mixed convection analysis of laminar pulsating flow and heat transfer over a backward-facing step. *International Journal of Heat and Mass Transfer*, 51:5785–5793, 2008.

[29] B. S. Alshuraiaan. Mixed convection flow and heat transfer over different geometries of backward-facing step. *Journal of Engineering Research*, 1:211–233, 2013.

[30] S. Acharya, G. Dixit, and Q. Hou. Laminar mixed convection in a vertical channel with a backstep: a benchmark study. *ASME Heat Transfer Division*, 258:11–20, 1993.

[31] J. Lin, B. Armaly, and T. Chen. Mixed convection in buoyancy-assisted vertical backward-facing step flows. *International Journal of Heat and Mass Transfer*, 33:2121–2132, 1990.